

Ternary Stochastic Geometry Theory for Performance Analysis of RIS-Assisted UDN

Hong-Chi Lin, *IEEE Student Member*, and Qi-Yue Yu[†], *IEEE Senior Member*

Abstract

With the fast development of reconfigurable intelligent surface (RIS), the network topology becomes more complex and varied, which makes the network design and analysis extremely challenging. Most of the current works adopt the binary system stochastic geometric, missing the coupling relationships between the direct and reflected paths caused by RISs. In this paper, we first define the typical triangle which consists of a base station (BS), a RIS and a user equipment (UE) as the basic ternary network unit in a RIS-assisted ultra-dense network (UDN). In addition, we extend the Campbell's theorem to the ternary system and present the ternary probability generating functional (PGFL) of the stochastic geometry. Based on the ternary stochastic geometry theory, we derive and analyze the coverage probability, area spectral efficiency (ASE), area energy efficiency (AEE) and energy coverage efficiency (ECE) of the RIS-assisted UDN system. Simulation results show that the RISs can improve the system performances, especially for the UE who has a high signal to interference plus noise ratio (SINR), as if the introduced RIS brings in Matthew effect. This phenomenon of RIS is appealing for guiding the design of complex networks.

Index Terms

Ultra-dense network, reconfigurable intelligent surface, ternary network system, typical triangle, ternary Campbell's theorem, ternary probability generating functional, energy coverage efficiency.

H.-C. Lin (email: linhongchi@stu.hit.edu.cn) and Q.-Y. Yu (email: yuqiye@hit.edu.cn) are with the Communication Research Center, Harbin Institute of Technology, China.

The work presented in this paper was supported by the National Natural Science Foundation of China under Grand No. 62071148 and No. 62171151, and partly by the Fundamental Research Funds for Central Universities under Grand No. HIT.OCEF.2021012.

I. INTRODUCTION

Currently, an innovative network architecture that can boost both network capacity and coverage is the reconfigurable intelligent surface (RIS) assisted ultra-dense network (UDN). Due to the well-behaved performances of RIS, i.e., low cost, low power consumption and easy installation, it may greatly mitigate UDN high energy consumption and densification. Thus, RIS-assisted UDN is regarded as one of the future network evolution paradigms for the coming 6G [1].

The emergence of RIS-assisted network may bring intricate network topologies and challenging network performance analysis. An efficient performance analysis manner for random networks is through stochastic geometry, which can provide a tight lower bound of the actual network simulation on a space-time averaging view [2]. However, the current stochastic geometry focuses on the theoretical architecture of binary system, whose two components are base station (BS) and user equipment (UE). Although many articles have analyzed and discussed multi-layer heterogeneous networks, they are still binary systems which do not consider the location relationship between macro and micro BSs [3]–[7]. Besides, stochastic geometry has been used for analyzing the relay systems, which can be viewed as the multi-segment binary systems [8]–[12]. With the complexity and variability of the communication requirements, the BS functions have gradually evolved into segmentation and marginalization, resulting in the emergence of different functional network units, such as RIS, caching unit, sensing unit and computing unit. Therefore, the future network topology will no longer be limited to the binary system architecture (focusing on points and lines), but evolve to multi-unit system architectures (focusing on planes and solids).

Coincidentally, the RIS-assisted UDN system is a typical ternary system. Some studies have investigated the RIS-assisted UDN system based on stochastic geometry [13]–[23]. Initially, it is assumed that the direct and reflected paths are completely separated by different working modes [13] and orthogonal time-frequency resources [14]. In [15] and [16], the authors applied the line of sight (LoS) indicator function to model the relationship between the direct link and the reflected link. [17] modeled the line Boolean blockages model to analyze the direct case and the reflection case. Subsequently, it is assumed that the received signal's direct and reflected paths might be independent from a receive diversity perspective [18]. Based on the approximation of statistical analysis, the direct and reflected paths can be roughly regarded as independent [19], [20]. The authors treat BS, RIS and UE as an equilateral triangle to make system analysis

simple in [21]. In [22], the authors calculated the successful reflection probability as well as the distribution of the distance by a line segment object model. By triangulation modeling, the authors in [23] incorporate reflection probability into the measurement analysis.

In summary, most of the current literatures on RIS networks analysis still adopt the binary system stochastic geometric, without fully considering the coupling relationships between the direct and reflected paths. However, for multi-unit system, it is crucial to use the geometric relationships among different network units to frame the system performance. Therefore, we propose a ternary stochastic geometric theory for the RIS-assisted UDN, and define a typical triangle to analyze the ternary network framework. Based on the typical triangle, we deduce and analyze a more comprehensive performance analysis of the RIS-assisted UDN system, as listed in Table I. The major contributions of this paper are three-fold:

- 1) We propose a ternary homogeneous Poisson point process to model the RIS-assisted UDN system, and give a comprehensive analysis and signal transmission process. To highlight the limitation of the RIS regulation signal, the RIS phase matrix maximizes the reflected signals in the absence of coordinated interferences;
- 2) We construct a ternary stochastic geometric basis, and define a typical triangle for analyzing the RIS-assisted UDN system. According to the geometric relationship of the typical triangle, we analyze the attribution relationship, distance distribution, and RIS reflection state, for analyzing the relationships among the edges/angles in the ternary system.
- 3) We propose the ternary Campbell's theorem and ternary probability generating functional (PGFL) of the stochastic geometry for analyzing the ternary network framework. Then, we derive and analyze the approximative closed formulae of signal statistical characteristics, coverage probability, area spectral efficiency (ASE) and area energy efficiency (AEE) in the RIS-assisted UDN system. More importantly, we define and derive the energy coverage efficiency (ECE) in the RIS-assisted UDN system.

The remainder of this paper is organized as follows. In Section II, we present the system model, including the signal transmission model and the design of the phase matrix of RIS. Based on stochastic geometry, Section III presents a typical triangle concept for analyzing RIS-assisted UDN. The theoretical analyses are deduced in Section IV. Simulation results are presented in Section V, followed by concluding remarks drawn in Section VI.

TABLE I: Comparisons between classical UDN and RIS-assisted UDN.

		UDN	RIS-assisted UDN
Theoretical basis	Voronoi diagram	ones/two point process (binary system)	multiple point process (ternary system)
	reference point	typical UE/BS	typical triangle
	Campbell's theorem	[3], [24], [25]	(19)
	probability generating functional	[3], [24], [25]	(22)
System model	signal transmission	[3], [5], [8], [24], [25]	(2), (18)
Application	signal statistics	[3], [22], [24], [25]	(25), (26)
	cover probability/ASE/AEE	[3]–[12], [24], [25], [29]	(30)/(33)/(34)
	ECE	/	(35)

II. SYSTEM MODEL

In this paper, a and \mathbf{A} respectively stand for a scalar and a matrix. Define the real number set and complex number set by \mathbb{R} and \mathbb{C} , respectively. $\mathcal{P}(\lambda)$ is Poisson distribution with parameter λ . $\mathcal{N}(\mu, \sigma^2)$ and $\mathcal{CN}(\mu, \sigma^2)$ are Gaussian distribution and complex Gaussian distribution with mean μ and variance σ^2 , respectively. Let $E[\cdot]$ and $D[\cdot]$ be the mean and variance of a random variable. Define $\text{diag}[a_1, a_2, \dots, a_n]$ by a diagonal matrix whose main diagonal elements are a_1, a_2, \dots, a_n in order. The superscripts of the matrix \mathbf{A}^T and \mathbf{A}^* respectively represent the transpose and conjugate of a matrix \mathbf{A} .

A. Signal transmission model

Assume that the distributions of BSs, RISs and UEs are homogeneous Poisson point processes (HPPPs) defined by Λ_N , Λ_M and Λ_U , with intensities λ_n , λ_m and λ_u , respectively. The number of BSs, RISs and UEs in the given area are respectively defined by N , M and U , where the area is modeled as a circle with radius R . According to the point generation process of HPPP [24], it is known that the number of points obeys Poisson distribution, while the locations of points obey uniform distribution in the given area. For example, the number of points N in Λ_N obeys Poisson distribution $\mathcal{P}(\lambda_n \pi R^2)$ and the locations of points are generated in the polar coordinate system by a “radial generation” method, i.e., the probability density function (PDF) of polar diameter is $f(x) = 2x/R^2$ ($0 \leq x \leq R$), and the polar angle θ obeys uniform distribution on $[0, 2\pi)$.

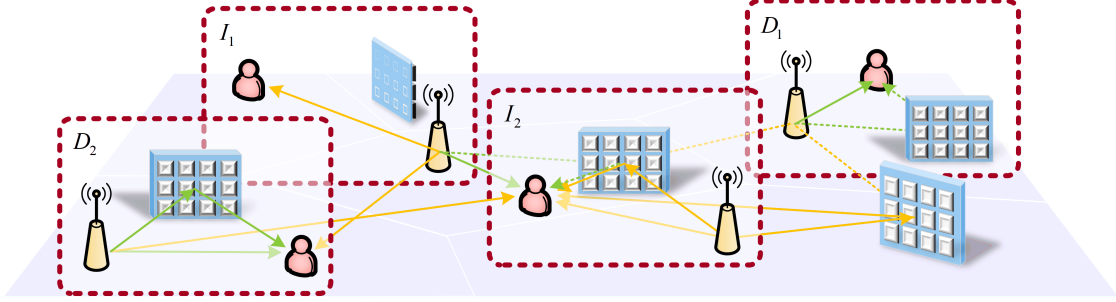


Fig. 1: Signal transmission diagram of RIS-assisted UDN, where D_1, D_2, I_1 and I_2 respectively stand for the direct signal, the reflection signal, the direct interference and the reflection interference.

This paper considers the narrow-band communication, which ignores the effect of transmission delay differences coming from the different electromagnetic waves. Let each equipment terminal (e.g., BS, and UE) hold one antenna, and each RIS has Q reflection elements. In addition, the RIS is assumed to reflect electromagnetic waves by only one side with the tunable phase, without considering the tunable amplitude [13], [14], [17], [22]. This paper mainly considers the downlink scenario of RIS-assisted UDN, with the assumption that each BS can only support up to one UE transmission [13], [14], [19], [20]. With the densification of BSs, the BS likely serves only one UE to control the coverage and service of each BS more precisely. Taking the n th BS as an example to analyze the transmission process, it is assumed that the u th UE is served by the n th BS, and the set of RISs serving the n th BS is defined by Ψ_n^M . Let the modulated signals of the u th UE be x_u , where $\text{E}[|x_u|^2] = 1$. Then, the transmit signal of the n th BS is expressed as

$$s_n = \sqrt{P_{tr}} x_u, \quad (1)$$

where P_{tr} is the transmit power of the n th BS, which is a constant for all the BSs.

The channel impulse response between the n th BS and the u th UE is denoted as $h_{n,u} \in \mathbb{C}$, the channel impulse response between the n th BS and the m th RIS is set to $\mathbf{w}_{n,m} = [w_{n,m,1}, w_{n,m,2}, \dots, w_{n,m,Q}]^T \in \mathbb{C}^{Q \times 1}$, and the channel impulse response between the m th RIS and the u th UE is set to be $\mathbf{g}_{m,u} = [g_{m,u,1}, g_{m,u,2}, \dots, g_{m,u,Q}] \in \mathbb{C}^{1 \times Q}$. Moreover, the reflection matrix of the m th RIS is defined by $\Phi_m \triangleq \text{diag}[\phi_{m,1}, \phi_{m,2}, \dots, \phi_{m,Q}]$, where $\phi_{m,q}$ is the controllable phase shift of the q th reflection element. The distance between the n th BS and the u th UE is defined by $d_{n,u}^D$, the distance between the n th BS and the m th RIS is defined by $d_{n,m}^I$, and the distance between the m th RIS and the u th UE is $d_{m,u}^R$, where the subscripts “D”, “I”, and “R” indicate “direct”, “incident” and “reflection”, respectively.

In this paper, the small-scale fading channels are modeled as complex Gaussian distribution $\mathcal{CN}(0, \sigma_h^2)$, and the large-scale fading channel only considers the bounded path loss model, i.e.,

$(1+d)^{-\alpha}$, where α is the path loss coefficient and d indicates the signal transmission distance. For the subsequent analysis, the path loss coefficient is set to be $\alpha = 4$. Therefore, the received signal of the u th UE is

$$\begin{aligned}
y_u &= \sum_{n=1}^N (1+d_{n,u}^D)^{-2} \cdot h_{n,u} s_n + \sum_{m=1}^M (1+d_{m,u}^R)^{-2} \cdot \mathbf{g}_{m,u} \Phi_m \left(\sum_{n=1}^N (1+d_{n,m}^I)^{-2} \cdot \mathbf{w}_{n,m} \beta_{n,m,u} s_n \right) + z_u \\
&= \underbrace{(1+d_{n,u}^D)^{-2} \cdot h_{n,u} s_n}_{D_1} + \underbrace{\sum_{m=1}^M (1+d_{m,u}^R)^{-2} (1+d_{n,m}^I)^{-2} \cdot \mathbf{g}_{m,u} \Phi_m \mathbf{w}_{n,m} \beta_{n,m,u} s_n}_{D_2} \\
&\quad + \underbrace{\sum_{\substack{n' \neq n, \\ n'=1}}^N (1+d_{n',u}^D)^{-2} \cdot h_{n',u} s_{n'}}_{I_1} + \underbrace{\sum_{m=1}^M (1+d_{m,u}^R)^{-2} \cdot \mathbf{g}_{m,u} \Phi_m \left(\sum_{\substack{n' \neq n, \\ n'=1}}^N (1+d_{n',m}^I)^{-2} \cdot \mathbf{w}_{n',m} \beta_{n',m,u} s_{n'} \right)}_{I_2} + z_u,
\end{aligned} \tag{2}$$

where $z_u \sim \mathcal{N}(0, \sigma_n^2)$ is the additive white Gaussian noise (AWGN) of the u th UE and $\beta_{n,m,u} \in \{0, 1\}$ represents the reflection state of the reflection signals from the n th BS through the m th RIS to the u th UE. If $\beta_{n,m,u} = 1$, the m th RIS can reflect the signals from the n th BS to the u th UE; otherwise, the interrupted link indicates that the RIS is inoperative. The first term of (2) defined by D_1 is the signal of the u th UE from the n th BS; the second term defined by D_2 is the signals of the u th UE from RISs; the third term and the fourth term respectively represent the interferences from other BSs and RISs, defined by I_1 and I_2 , as shown in Fig. 1.

For further discussion, the cascade channel impulse response from the n th BS through the m th RIS to the u th UE is defined by $h_{n,m,u} = \mathbf{g}_{m,u} \Phi_m \mathbf{w}_{n,m}$. Thus, the signal to interference plus noise ratio (SINR) of the u th UE γ_u is given by

$$\gamma_u = \frac{P_{tr} \left| (1+d_{n,u}^D)^{-2} \cdot h_{n,u} + \sum_{m=1}^M (1+d_{m,u}^R)^{-2} (1+d_{n,m}^I)^{-2} \cdot h_{n,m,u} \beta_{n,m,u} \right|^2}{P_{tr} \sum_{\substack{n' \neq n, \\ n'=1}}^N (1+d_{n',u}^D)^{-4} \cdot |h_{n',u}|^2 + P_{tr} \sum_{m=1}^M (1+d_{m,u}^R)^{-4} \cdot \left(\sum_{\substack{n' \neq n, \\ n'=1}}^N (1+d_{n',m}^I)^{-4} \cdot |h_{n',m,u}|^2 \beta_{n',m,u}^2 \right) + \sigma_n^2}, \tag{3}$$

where the cascade channel impulse response $h_{n,m,u}$ has a significant impact on D_2 and I_2 , especially for the gain of combining signals of the UE. Therefore, we can design the phase matrix Φ_m of RIS, so that the cascade channel can be indirectly controlled to the maximum modulus state.

B. Design of the phase matrix of RIS

Since this paper only considers the phase tuning capability of RIS, the phase matrixs of RISs are designed to maximize the power of signals. Thus, the controllable phase shift of the q th

reflection element of the m th RIS is

$$\phi_{m,q} = \frac{h_{n,u}}{|h_{n,u}|} \cdot \frac{w_{n,m,q}^*}{|w_{n,m,q}|} \cdot \frac{g_{m,u,q}^*}{|g_{m,u,q}|}, \quad 1 \leq q \leq Q, \quad m \in \Psi_n^M, \quad (4)$$

where $\phi_{m,q}$ is determined by the product of three parts, i.e., the phase of $h_{n,u}$, $w_{n,m,q}^*$ and $g_{m,u,q}^*$.

Consequently, the cascade channel gain from the n th BS through the m th RIS to the u th UE is expressed as

$$|h_{n,m,u}^C| = \begin{cases} \sum_{q=1}^Q |g_{m,u,q}| \cdot |w_{n,m,q}|, & m \in \Psi_n^M, \\ \left| \sum_{q=1}^Q g_{m,u,q} \cdot w_{n,m,q} \right|, & m \notin \Psi_n^M, \end{cases} \quad (5)$$

where $m \notin \Psi_n^M$ indicates that the m th RIS does not serve the n th BS. According to [20], if $m \in \Psi_n^M$, the phase matrix Φ_m is matched with the channel impulse response $\mathbf{w}_{n,m}$ and $\mathbf{g}_{m,u}$, and the reflection signals can be aligned. Thus, the PDF of $h_{n,m,u}$ is approximately a Gaussian distribution, i.e., $\mathcal{N}\left(\frac{\pi}{2}Q\sigma_h^2, (4 - \frac{\pi^2}{4})Q\sigma_h^4\right)$. In contrast, if $m \notin \Psi_n^M$, the reflection signals become random variables to the u th UE, so that the PDF of $h_{n,m,u}$ is approximately a complex Gaussian distribution $\mathcal{CN}(0, 2Q\sigma_h^4)$.

In the following, the interrelationships among the three HPPPs are analyzed through the classical stochastic geometry theories, and their relative distance probability distributions are combed out for calculating the large-scale fading. Additionally, the reflection state of RIS is modeled by relative distance analysis.

III. GEOMETRIC MODEL FOR RIS-ASSISTED UDN

A typical point (BS or UE) is generally specified at the classical stochastic geometry theory for evaluating the performance of the entire network, since the Slivnyak Theorem has proved that the statistical characteristics of HPPP are independent of the location of the observation point [25]. Moreover, the traditional point-to-point communication only concerns the relative distance between the BS and UE. Nevertheless, the RIS-assisted UDN system is a ternary system, which consists of three points, namely one BS, one RIS, and one UE, forming a triangle $\triangle BRU$ geometric relationship. To represent the geometry relationships of the three points, this section proposes the typical triangle as the ternary stochastic geometric basis.

A. Multiple voronoi diagrams

In stochastic geometry, the voronoi diagram is frequently used for describing cell distribution. Through the vertical intersection of two nearby points, it divides the region into several voronoi

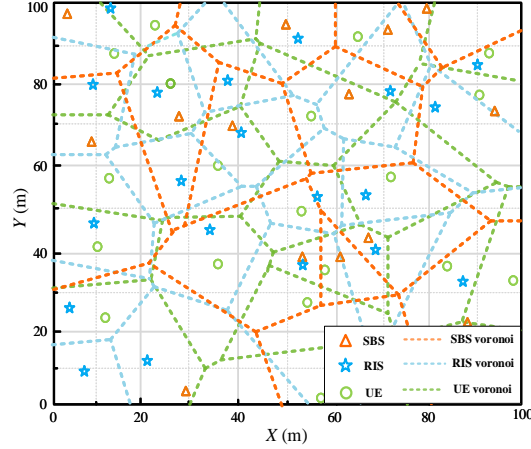


Fig. 2: The voronoi diagram of a RIS-assisted UDN, where $N = 15$, $M = 20$ and $U = 20$.

cells. There are three types of nodes for the RIS-assisted UDN: BS nodes, RIS nodes, and UE nodes. As a result, three different voronoi diagram types are taken into account. An illustration of the voronoi diagram for a RIS-assisted UDN system is shown in Fig. 2, where $N = 15$, $M = 20$, and $U = 20$. It is found that the voronoi diagrams of the BS, RIS and UE may appear to overlap, which exacerbates the difficulty of analyzing multiple voronoi diagrams.

It is known that the PDF of the area of voronoi cell has been given as

$$f_{X_B}(x_b) = \frac{3.5^{3.5}}{\Gamma(3.5)} x_b^{2.5} e^{-3.5x_b}, \quad (6)$$

where x_b is the random variable that reflects the normalized voronoi cell area of BS [26].

Referring to the proposed method in [27], we can obtain the probability of RISs and UEs located in the voronoi cell of BS. Assume there are m RISs and u UEs in the voronoi cell of a given BS, where $0 \leq m \leq M$ and $0 \leq u \leq U$, whose probability is calculated as

$$\begin{aligned} P[\mathcal{M} = m, \mathcal{U} = u] &\stackrel{(a)}{=} \int_0^\infty \frac{\left(\lambda_m \frac{x_b}{\lambda_n}\right)^m}{m!} e^{-\lambda_m \frac{x_b}{\lambda_n}} \cdot \frac{\left(\lambda_u \frac{x_b}{\lambda_n}\right)^u}{u!} e^{-\lambda_u \frac{x_b}{\lambda_n}} \cdot f_{X_B}(x_b) dx_b \\ &= \frac{3.5^{3.5} \Gamma(m+u+3.5) \left(\frac{\lambda_m}{\lambda_n}\right)^m \left(\frac{\lambda_u}{\lambda_n}\right)^u}{m! u! \Gamma(3.5) \left(\frac{\lambda_m + \lambda_u}{\lambda_n} + 3.5\right)^{m+u+3.5}}, \end{aligned} \quad (7)$$

where (a) is deduced based on the fact that Λ_M and Λ_U are independent point processes.

Thus, the probability of at least one RIS and one UE located in the BS voronoi cell is

$$P[m \neq 0, u \neq 0] = 1 - \left(1 + \frac{\lambda_u}{3.5\lambda_n}\right)^{-3.5} - \left(1 + \frac{\lambda_m}{3.5\lambda_n}\right)^{-3.5} + \left(1 + \frac{\lambda_m + \lambda_u}{3.5\lambda_n}\right)^{-3.5}. \quad (8)$$

When $\lambda_m = 0$, the probability of at least one UE located in the BS voronoi cell is

$$P[u \neq 0] = 1 - \left(1 + \frac{\lambda_u}{3.5\lambda_n}\right)^{-3.5}, \quad (9)$$

where $P[u \neq 0]$ is usually considered as the probability of an active BS [27]. According to the thinning theorem of HPPP [24], [25], the intensity of active BS is $\lambda'_{un} \triangleq P[u \neq 0] \lambda_n$.

After previous analysis, it can be found that the RISs are split into two types: inside the reference BS voronoi cell, i.e., $m \in \Psi_n^M$ and outside the reference BS voronoi cell, i.e., $m \notin \Psi_n^M$, depending on the distance relationship between the RISs and the reference BS. The RISs inside the voronoi cell are capable of beamforming, while the RISs outside the cell are unable to align with the signals. This leads to the fact that the Poisson point process Λ_M is split into two parts due to the different measurable functions. Furthermore, the distances from the RISs in the voronoi cell to the reference BS are both smaller than that of the RISs outside the voronoi cell, i.e., $d_{n,m}^I \leq d_{n,m'}^I, m \in \Psi_n^M, m' \notin \Psi_n^M$. It is worth noting that for the RIS-assisted UDN system, we cannot refine the analysis by the thinning RIS intensity process. Therefore, this paper adopts a dual-intensity analysis mode of RIS and active BS to analyze the specific interrelationships in the RIS-assisted UDN system.

B. Typical \triangle BRU

Let the typical BS locate at the origin and construct its voronoi cell. Define the nearest UE to the typical BS as the typical UE. Since this paper assumes that the BS only serves the nearest UE, it becomes essential to analyze the distance orders of all the UEs. Therefore, we redefine the n th BS serial number n to indicate the n th closest BS to the typical UE, and the typical BS is defined as the 1st BS. Similarly, the u th UE serial number u means that it is the u th closest distance away from the typical BS, and the typical UE is defined as the 1st UE. The m th RIS serial number m indicates that it is the m th closest distance to the typical BS. According to the Slivnyak Theorem and the characteristics of HPPP, it is known that the observation position does not affect the relative distance. Therefore, the relative distances can be observed from the perspective of the typical BS or the typical UE. Furthermore, we define a “BRU-triangle” with at least one typical point (BS or UE) as a typical \triangle BRU.

Fig. 3 shows a schematic analysis of a typical \triangle BRU from a 3D and 2D view, respectively. As shown in Fig. 3(b), two coordinate systems are established by setting the typical BS and the typical UE as the origin points, respectively. From the perspective of the typical BS (located at the origin), it is derived that the PDF of $d_{1,m}^I$ as follows

$$f(d_{1,m}^I) = \frac{2(\pi\lambda_m)^m}{(m-1)!} (d_{1,m}^I)^{2m-1} \cdot e^{-\pi\lambda_m(d_{1,m}^I)^2}. \quad (10)$$

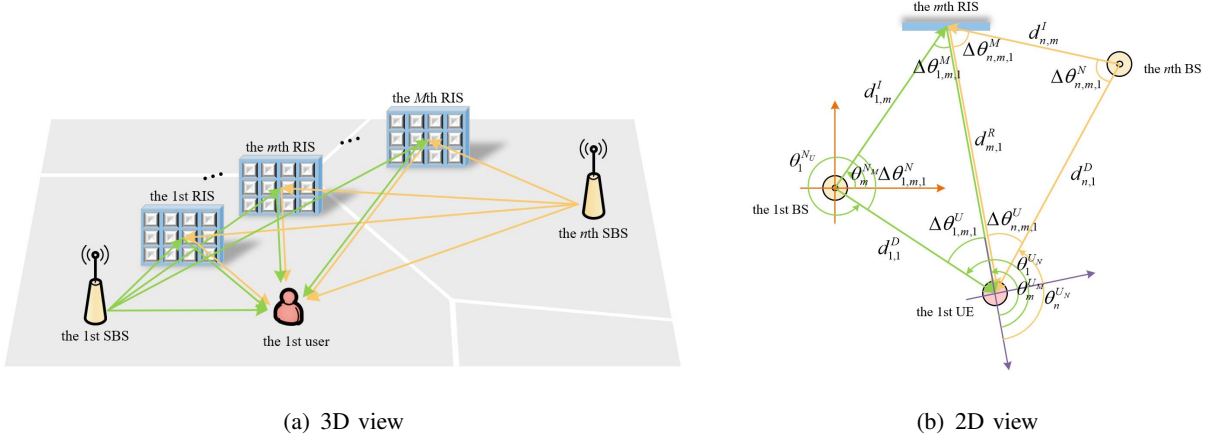


Fig. 3: The geometric relationship of the typical Δ BRU. (a) is a global 3D view, and (b) is the m th RIS 2D view.

Define the function $f_{\lambda,i}(x)$ by $f_{\lambda,i}(x) = \frac{2(\pi\lambda)^i}{(i-1)!} x^{2i-1} e^{-\pi\lambda x^2}$, so that the PDF of $d_{1,m}^I$ shown in (10) can be represented by $f_{\lambda_m,m}(d_{1,m}^I)$. In addition, we can also find that the typical BS's vertex angle $\Delta\theta_{1,m,1}^N = \theta_m^{N_M} - \theta_1^{N_U}$ obeys the uniform distribution in the range of $[0, 2\pi)$, since the polar angle $\theta_m^{N_M}$ and $\theta_1^{N_U}$ are i.i.d. and both obey the uniform distribution on $[0, 2\pi)$.

Similarly, from the perspective of the typical UE (which is located at the origin), the PDF of $d_{n,1}^D$ is expressed as $f_{\lambda'_{un,n}}(d_{n,1}^D)$. Thus, the PDF of the distance between the typical UE and the typical BS can be expressed as

$$f(d_{1,1}^D) = 2\pi\lambda'_{un} d_{1,1}^D \cdot e^{-\pi\lambda'_{un} (d_{1,1}^D)^2}. \quad (11)$$

Although from the perspective of the typical BS, $\theta_m^{U_M}$ does not obey the uniform distribution because of the intra-triangular coupling relationships. However, from the perspective of the typical UE, $\theta_n^{U_N}$ is independent of $\theta_m^{U_M}$, so that the typical UE's vertex angle $\Delta\theta_{n,m,1}^U = \theta_m^{U_M} - \theta_n^{U_N}$ is still uniform distribution on $[0, 2\pi)$ for a given $\theta_m^{U_M}$, as shown in Fig. 3(b).

According to the law of cosines, it can be obtained that

$$d_{m,1}^R = \sqrt{(d_{1,1}^D)^2 + (d_{1,m}^I)^2 - 2d_{1,1}^D d_{1,m}^I \cos(\Delta\theta_{1,m,1}^N)}.$$

Thus, by changing variables, the PDF of $d_{m,1}^R$ is deduced as

$$f(d_{m,1}^R) = \int_0^\infty \int_{|d_{1,1}^D - d_{m,1}^R|}^{d_{1,1}^D + d_{m,1}^R} \frac{d_{m,1}^R}{\pi d_{1,1}^D d_{1,m}^I \sqrt{1 - \left(\frac{(d_{1,1}^D)^2 + (d_{1,m}^I)^2 - (d_{m,1}^R)^2}{2d_{1,1}^D d_{1,m}^I} \right)^2}} f(d_{1,m}^I) f(d_{1,1}^D) dd_{1,m}^I dd_{1,1}^D. \quad (12)$$

When $m = 1$, the PDF of $d_{1,1}^R$ can be deduced as

$$\begin{aligned}
f(d_{1,1}^R) &\stackrel{(a)}{=} \int_0^\infty \int_{-1}^1 \frac{2\lambda_m d_{1,1}^R}{\sqrt{1-x^2}} \cdot e^{-\pi\lambda_m [(d_{1,1}^D)^2 + (d_{1,1}^R)^2 - 2d_{1,1}^D d_{1,1}^R x]} dx f(d_{1,1}^D) dd_{1,1}^D \\
&\stackrel{(b)}{=} \int_0^\infty 2\lambda_m d_{1,1}^R e^{-\pi\lambda_m [(d_{1,1}^D)^2 + (d_{1,1}^R)^2]} \cdot \pi I_0(2\pi\lambda_m d_{1,1}^D d_{1,1}^R) \cdot f(d_{1,1}^D) dd_{1,1}^D \\
&= 2\pi \frac{\lambda_m \lambda'_{un}}{\lambda_m + \lambda'_{un}} d_{1,1}^R e^{-\pi \frac{\lambda_m \lambda'_{un}}{\lambda_m + \lambda'_{un}} (d_{1,1}^R)^2},
\end{aligned} \tag{13}$$

where (a) is deduced by $x = \frac{(d_{1,1}^D)^2 + (d_{1,1}^R)^2 - (d_{1,1}^I)^2}{2d_{1,1}^D d_{1,1}^R}$; and (b) is relayed on the integral function table in [28].

Similarly, by deducing and checking the integration table, the expressions of the cases $m = 2$ and $m = 3$ can be obtained as

$$f(d_{2,1}^R) = \frac{\lambda_m}{\lambda_m + \lambda'_{un}} f_{\lambda^*,1}(d_{2,1}^R) + \frac{\lambda'_{un}}{\lambda_m + \lambda'_{un}} f_{\lambda^*,2}(d_{2,1}^R), \tag{14a}$$

$$f(d_{3,1}^R) = \frac{\lambda_m^2}{(\lambda_m + \lambda'_{un})^2} f_{\lambda^*,1}(d_{3,1}^R) + \frac{2\lambda'_{un}\lambda_m}{(\lambda_m + \lambda'_{un})^2} f_{\lambda^*,2}(d_{3,1}^R) + \frac{\lambda'^2_{un}}{(\lambda_m + \lambda'_{un})^2} f_{\lambda^*,3}(d_{3,1}^R), \tag{14b}$$

where $\lambda^* = \frac{\lambda'_{un}\lambda_m}{\lambda'_{un} + \lambda_m}$ is defined as the coupling intensity of two HPPPs Λ'_{UN} and Λ_M .

Hence, through inductive reasoning, the PDF of $d_{m,1}^R$ can be obtained as

$$\begin{aligned}
f(d_{m,1}^R) &= \sum_{i=1}^m C_{m-1}^{i-1} \left(\frac{\lambda_n}{\lambda_m + \lambda_n} \right)^{i-1} \left(\frac{\lambda_m}{\lambda_m + \lambda_n} \right)^{m-i} \frac{2}{(i-1)!} \left(\pi \frac{\lambda_m \lambda'_{un}}{\lambda_m + \lambda'_{un}} \right)^i (d_{m,1}^R)^{2i-1} e^{-\pi \frac{\lambda_m \lambda'_{un}}{\lambda_m + \lambda'_{un}} (d_{m,1}^R)^2} \\
&= \sum_{i=1}^m C_{m-1}^i (p_m^*)^{i-1} (p_n^*)^{m-i} f_{\lambda^*,i}(d_{m,1}^R),
\end{aligned} \tag{15}$$

where $p_m^* = \frac{\lambda_m}{\lambda_m + \lambda'_{un}}$ and $p_n^* = \frac{\lambda'_{un}}{\lambda_m + \lambda'_{un}}$ can be understood as the ratio of the coupling intensity with λ_m and λ'_{un} . To further illustrate the physical meaning of (15), we define the Poisson pair to describe the coupling relationship of two HPPPs, and give the intensity of the Poisson pair.

Definition 1 (Poisson pair). *The intensities of two given HPPPs Λ_1 and Λ_2 are λ_1 and λ_2 , respectively. o_1 denotes any point in the HPPP Λ_1 , and o_2 denotes any point in the HPPP Λ_2 . If o_1 is exactly within the voronoi cell of o_2 , and o_2 is also exactly within the voronoi cell of o_1 , we define these two points as a Poisson pair (Λ_1, Λ_2) , and the intensity of the Poisson pair satisfies exactly $\frac{1}{\lambda^*} = \frac{1}{\lambda_1} + \frac{1}{\lambda_2}$, i.e., $\lambda^* = \frac{\lambda_1 \lambda_2}{\lambda_1 + \lambda_2}$.*

Proof. According to (11), if o_1 is within the voronoi cell of o_2 , the PDF of the distance between o_1 and o_2 is $f_{\lambda_1,1}(x) = 2\pi\lambda_1 x \cdot \exp(-\pi\lambda_1 x^2)$. At this time, the conditional probability of that o_2 is within the voronoi cell of o_1 given x is $1 - e^{-\pi\lambda_2 x^2}$. Thus, the intensity λ^* of the Poisson pair (Λ_1, Λ_2) can be expressed as

$$\lambda^* = \lambda_1 \int_0^\infty (1 - e^{-\pi\lambda_2 x^2}) 2\pi\lambda_1 x e^{-\pi\lambda_1 x^2} dx = \frac{\lambda_1 \lambda_2}{\lambda_1 + \lambda_2}. \tag{16}$$

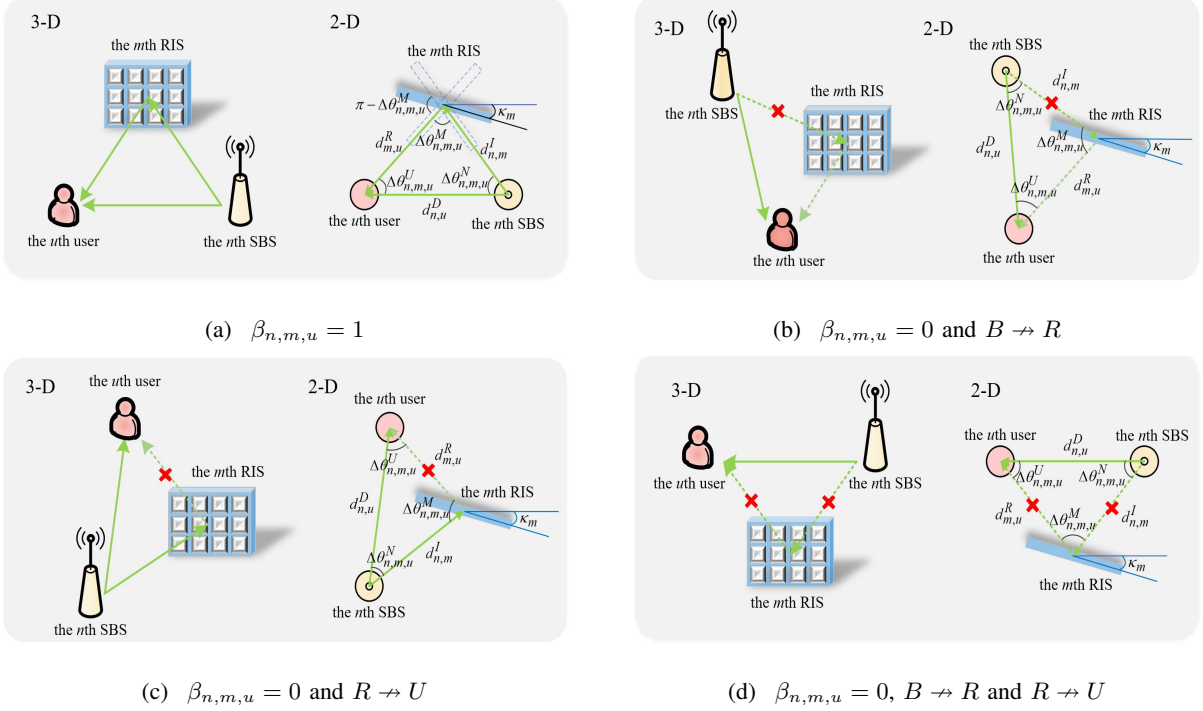


Fig. 4: Diagram of four reflection cases in the network, where “solid line” represents the transmission link and “dashed line” represents the interrupted link. (a) full connection; (b) the interrupted link, i.e., $B \nrightarrow R$; (c) the interrupted link, i.e., $R \nrightarrow U$; (d) the interrupted link, i.e., $B \nrightarrow R \nrightarrow U$.

□

Therefore, the intensity of the Poisson pair $(\Lambda'_{UN}, \Lambda_M)$ of (15) is determined by two HPPPs Λ'_{UN} and Λ_M , namely $\lambda^* = \frac{\lambda_m \lambda'_{un}}{\lambda_m + \lambda'_{un}}$.

C. Mathematic model of the reflection state of a RIS

The $\triangle BRU$ consists of three transmission links (or called sides), which are from BS to RIS, i.e., $B \rightarrow R$, from BS to UE, i.e., $B \rightarrow U$, and from RIS to UE, i.e., $R \rightarrow U$. This paper assumes that the interrupted link is generated by the placement angle κ_m of the RIS, because of the one-side reflection. Let $\beta_{n,m,u} \in \{0, 1\}$ be the reflection state of the RIS. If $\beta_{n,m,u} = 1$, the m th RIS can reflect the signals from the n th BS to the u th UE; otherwise, the interrupted link indicates that the RIS does not work and $\beta_{n,m,u} = 0$. Thus, there are generally four cases: full connection, the interrupted link of $B \nrightarrow R$, the interrupted link of $R \nrightarrow U$, and the interrupted link of $B \nrightarrow R \nrightarrow U$, as shown in Fig. 4.

According to the geometric relationship of $\triangle\text{BRU}$, the successful reflection placement angle range is from $-\theta_m^{NM}$ to $\pi - \Delta\theta_{n,m,u}^M - \theta_m^{NM}$, as shown in Fig. 4. Thus, the reflection state $\beta_{n,m,u}$ of the m th RIS is expressed as

$$\beta_{n,m,u} = \begin{cases} 1, & -\theta_m^{NM} \leq \kappa_m \leq \pi - \Delta\theta_{n,m,u}^M - \theta_m^{NM}, \\ 0, & \text{others,} \end{cases} \quad (17)$$

where θ_m^{NM} is the polar angle of the m th RIS and $\Delta\theta_{n,m,u}^M$ is the m th RIS's vertex angle.

Assume the placement angle of RIS κ_m obeys uniform distribution on $[0, 2\pi)$. Thus, for a given angle $\Delta\theta_{n,m,u}^M$, the conditional probability of $\beta_{n,m,u} = 1$ is calculated as

$$\text{P} \left[\beta_{n,m,u} = 1 \mid \Delta\theta_{n,m,u}^M \right] = \int_0^{2\pi} \int_{-\theta_m^M}^{\pi - \Delta\theta_{n,m,u}^M - \theta_m^M} f(\kappa_m) f(\theta_m^M) d\kappa_m d\theta_m^M = \frac{\pi - \Delta\theta_{n,m,u}^M}{2\pi} \leq \frac{1}{2}, \quad (18)$$

where $\Delta\theta_{n,m,u}^M = \arccos \left[\frac{(d_{m,u}^R)^2 + (d_{n,m}^I)^2 - (d_{n,u}^D)^2}{2d_{m,u}^R d_{n,m}^I} \right]$. It is found that the assumption that only half of the RIS intensity supports the reflection should be an upper bound of the exact value. So far, the PDFs of all sides, angles and reflection states in the typical $\triangle\text{BRU}$ have been deduced, which are used for further analyzing the distribution characteristics of the signals and system performance parameters of the RIS-assisted UDN system.

IV. TERNARY-SYSTEM STOCHASTIC GEOMETRIC ANALYSIS FOR RIS-ASSISTED UDN

In the previous section, we have analysed and discussed the attribution relationship, edges, angles and reflection probabilities in the RIS-assisted UDN system. Based on these analyses, this section firstly presents the ternary-system stochastic geometry theory, and then applies it to analyze the system performances in the RIS-assisted UDN system.

A. Ternary-system stochastic geometry theory

The stochastic geometry is widely used, since it can transform the mean form of random sum (Campbell's theorem) and random product (PGFL analysis) of point processes into an integral form, resulting in simplified computability and well-behaved analyticity [24]. Considering the RIS-assisted UDN system is a ternary network topology, the original Campbell's theorem and PGFL analysis cannot be directly applied into the ternary networks. Thus, we firstly propose the ternary-system stochastic geometry theory. Firstly, we propose Lemma 1 to obtain the mean of the ternary random sum in the RIS-assisted UDN.

Lemma 1 (Ternary Campbell's theorem). *A HPPP Λ with intensity λ is a point process on the two-dimensional plane \mathbb{R}^2 . $g_{s_1}(x)$ and $g_{s_2}(x)$ are respectively measurable functions of \mathcal{S}_1 and*

\mathcal{S}_2 , where \mathcal{S}_1 and \mathcal{S}_2 are the absolute complement of each other on \mathbb{R}^2 . Define the point process of Λ in \mathcal{S}_1 and in \mathcal{S}_2 by Λ_{s_1} and Λ_{s_2} , respectively. When $g_{s_1}(x)$ and $g_{s_2}(x)$ are respectively convergent in \mathcal{S}_1 and \mathcal{S}_2 , the mean value of the sum signal is denoted by

$$\mathbb{E} \left[\sum_{x \in \Lambda_{s_1}} g_{s_1}(x) + \sum_{x \in \Lambda_{s_2}} g_{s_2}(x) \right] = 2\pi\lambda \left(\int_{\mathcal{S}_1} g_{s_1}(x) dx + \int_{\mathcal{S}_2} g_{s_2}(x) dx \right). \quad (19)$$

Proof. \mathcal{S}_1 and \mathcal{S}_2 are the absolute complement of each other on \mathbb{R}^2 . Hence, suppose that there are k_1 points in \mathcal{S}_1 and k_2 points in \mathcal{S}_2 , satisfying $k_1 + k_2 = k$. Λ_{s_1} and Λ_{s_2} are two independent parts of Λ because \mathcal{S}_1 and \mathcal{S}_2 are the absolute complement of each other on \mathbb{R}^2 . Thus, the mean value of the random sum is

$$\begin{aligned} \mathbb{E} \left[\sum_{x \in \Lambda_{s_1}} g_{s_1}(x) + \sum_{x \in \Lambda_{s_2}} g_{s_2}(x) \right] &\stackrel{(a)}{=} \sum_{k_1=0}^{\infty} \mathbb{P}(k_1) \mathbb{E} \left[\sum_{x \in \Lambda_{s_1}} g_{s_1}(x) \mid |\Lambda_{s_1}| = k_1 \right] + \sum_{k_2=0}^{\infty} \mathbb{P}(k_2) \mathbb{E} \left[\sum_{x \in \Lambda_{s_2}} g_{s_2}(x) \mid |\Lambda_{s_2}| = k_2 \right] \\ &= 2\pi\lambda \left(\int_{\mathcal{S}_1} g_{s_1}(x) dx + \int_{\mathcal{S}_2} g_{s_2}(x) dx \right), \end{aligned} \quad (20)$$

where (a) is because Λ_{s_1} and Λ_{s_2} are independent. \square

In this paper, \mathcal{S}_1 is the area of the typical voronoi cell, whereas \mathcal{S}_2 is the area of the combination of other BS cells. According to the Bayes' theorem, the ternary Campbell's theorem in continuous variable form is expressed as

$$\mathbb{E} \left[\sum_{x \in \Lambda_{s_1}} g_{s_1}(x) + \sum_{x \in \Lambda_{s_2}} g_{s_2}(x) \right] = \int_0^{\infty} \mathbb{E} \left[\sum_{x \in \Lambda_{s_1}(x_b)} g_{s_1}(x) + \sum_{x \in \Lambda_{s_2}(x_b)} g_{s_2}(x) \mid x_b \right] f_{X_B}(x_b) dx_b, \quad (21)$$

which is very effective in subsequent applications.

Similarly, we derive Lemma 2 to analyze the PGFL of HPPP in the ternary-system.

Lemma 2 (Ternary PGFL analysis). *A HPPP Λ with intensity λ is a point process on \mathbb{R}^2 . $g_{s_1}(x)$ and $g_{s_2}(x)$ are respectively a measurable function in \mathcal{S}_1 and \mathcal{S}_2 , where \mathcal{S}_1 and \mathcal{S}_2 are the absolute complement of each other on \mathbb{R}^2 . Define the point process of Λ in \mathcal{S}_1 and in \mathcal{S}_2 by Λ_{s_1} and Λ_{s_2} , respectively. When $g_{s_1}(x)$ and $g_{s_2}(x)$ are respectively convergent in \mathcal{S}_1 and \mathcal{S}_2 , the mean value of the random product is denoted by*

$$\mathbb{E} \left[\prod_{x \in \Lambda_{s_1}} g_{s_1}(x) \prod_{x \in \Lambda_{s_2}} g_{s_2}(x) \right] = \exp \left(-2\pi\lambda \left(\int_{\mathcal{S}_1} (1 - g_{s_1}(x)) dx + \int_{\mathcal{S}_2} (1 - g_{s_2}(x)) dx \right) \right). \quad (22)$$

Proof. Similar to the definition of Lemma 1, the mean value of the random product is

$$\begin{aligned} \mathbb{E} \left[\prod_{x \in \Lambda_{s_1}} g_{s_1}(x) \prod_{x \in \Lambda_{s_2}} g_{s_2}(x) \right] &= \left(\sum_{k_1=0}^{\infty} \mathbb{P}(k_1) \mathbb{E} \left[\prod_{x \in \Lambda_{s_1}} g_{s_1}(x) \mid |\Lambda_{s_1}| = k_1 \right] \right) \cdot \left(\sum_{k_2=0}^{\infty} \mathbb{P}(k_2) \mathbb{E} \left[\prod_{x \in \Lambda_{s_2}} g_{s_2}(x) \mid |\Lambda_{s_2}| = k_2 \right] \right) \\ &= \exp \left(-2\pi\lambda \left(\int_{\mathcal{S}_1} (1 - g_{s_1}(x)) dx + \int_{\mathcal{S}_2} (1 - g_{s_2}(x)) dx \right) \right). \end{aligned} \quad (23)$$

\square

Similar to (21), the PGFL in continuous variable form can be expressed as

$$\mathbb{E} \left[\prod_{x \in \Lambda_{s_1}} g_{s_1}(x) + \prod_{x \in \Lambda_{s_2}} g_{s_2}(x) \right] = \int_0^\infty \mathbb{E} \left[\prod_{x \in \Lambda_{s_1}(x_b)} g_{s_1}(x) + \prod_{x \in \Lambda_{s_2}(x_b)} g_{s_2}(x) \middle| x_b \right] f_{X_B}(x_b) dx_b, \quad (24)$$

which is used for deriving the coverage probability and ASE.

B. Signal statistical characteristics

According to Lemma 1, the subsection deduces the statistical characteristics of the signals and the interferences.

1) *Signals*: In Appendix A, the detailed deduction processes of the power of the entire signal D_{sum} have been deduced, and the expressions is expressed as

$$\begin{aligned} \mathbb{E}[|D_{sum}|^2] = & P_{tr} \int_0^\infty \int_0^\infty \left\{ \left[\frac{\pi^3}{2} (Q-1) Q \sigma_h^4 \lambda_m \int_0^{\sqrt{\frac{x_b}{\pi \lambda'_{un}}}} \mathcal{Q} \left(\frac{1}{(1+d_{m,1}^R)^4 (1+d_{1,m}^I)^4} \right) d_{1,m}^I dd_{1,m}^I \right. \right. \\ & + \pi^4 Q^2 \sigma_h^4 \lambda_m^2 \left(\int_0^{\sqrt{\frac{x_b}{\pi \lambda'_{un}}}} \mathcal{Q} \left(\frac{1}{(1+d_{m,1}^R)^2 (1+d_{1,m}^I)^2} \right) d_{1,m}^I dd_{1,m}^I \right)^2 + \frac{2\sigma_h^2}{(1+d_{1,1}^D)^4} \\ & + \left. \frac{\sqrt{2\pi^5} Q \sigma_h^3 \lambda_m}{(1+d_{1,1}^D)^2} \int_0^{\sqrt{\frac{x_b}{\pi \lambda'_{un}}}} \mathcal{Q} \left(\frac{1}{(1+d_{m,1}^R)^2 (1+d_{1,m}^I)^2} \right) d_{1,m}^I dd_{1,m}^I \right] f_{X_B}(x_b) dx_b \\ & + 8\pi \lambda_m Q \sigma_h^4 \int_0^\infty \mathcal{Q} \left(\frac{1}{(1+d_{m,1}^R)^4 (1+d_{1,m}^I)^4} \right) d_{1,m}^I dd_{1,m}^I \left. \right\} f(d_{1,1}^D) dd_{1,1}^D, \end{aligned} \quad (25)$$

where $\mathcal{F}(a, k) \triangleq \int_0^\infty \frac{x}{(1+x)^a} e^{-kx^2} dx$, and $\mathcal{Q}(x) \triangleq \int_0^\pi \frac{P(\beta_{n,m,1}=1|\Delta\theta_{n,m,1}^M)}{\pi} x d\Delta\theta$. Note that, if $n = 1$, we set $\Delta\theta = \Delta\theta_{1,m,1}^N$; otherwise, if $n \neq 1$, $\Delta\theta = \Delta\theta_{n,m,1}^U$.

Observing (25), it can be found that $\mathbb{E}[|D_{sum}|^2] \geq \mathbb{E}[|D_1|^2] + \mathbb{E}[|D_2|^2]$, since the direct signal D_1 and the partial reflection signals with beamforming in D_2 can be superimposed in the same phase. When $\sqrt{\frac{x_b}{\pi \lambda'_{un}}} \xrightarrow{\lambda'_{un} \rightarrow \infty} 0$, the number of RISs in the typical voronoi cell becomes small. At this time, most of the RISs are not used for beamforming, so that the RIS plays a small role in enhancing signals in an extremely dense UDN system. This result will be proved in the following simulation section.

2) *Interferences*: Similarly, the power of the entire interference I_{sum} have been deduced detailedly in the Appendix B, and is expressed as

$$\begin{aligned} \mathbb{E}[|I_{sum}|^2] = & 4\pi P_{tr} \sigma_h^2 \lambda'_{un} \left[\frac{1}{6} - \mathcal{F}(4, \pi \lambda'_{un}) + 4Q\pi \lambda_m \sigma_h^2 \int_0^\infty \int_{d_{1,1}^D}^\infty \int_0^\infty \mathcal{Q} \left(\frac{1}{(1+d_{m,1}^R)^4 (1+d_{n',m}^I)^4} \right) \right. \\ & \left. d_{m,1}^R dd_{m,1}^R d_{n',1}^D dd_{n',1}^D f(d_{1,1}^D) dd_{1,1}^D \right]. \end{aligned} \quad (26)$$

According to (26), it can be found that $\mathbb{E}[|I_{sum}|^2] = \mathbb{E}[|I_1|^2] + \mathbb{E}[|I_2|^2]$, since I_1 and I_2 are independent of each other and have the complex Gaussian distributions with zero mean for their small-scale fadings. Furthermore, it is discovered that the power of I_2 is proportionality to $Q\lambda_m$.

C. Performance analysis

According to Lemma 2, we deduce the approximate closed formulas of coverage probability, ASE and energy efficiency of the RIS-assisted UDN system. In general, a linear approximation model has been widely employed to describe the power consumption of BS P_n and RIS P_m , i.e. $P_n = \Delta_p P_{tr} + P_{n_s}$ [23] and $P_m = Q P_{m_d} + P_{m_s}$ [31], where P_{n_s} and P_{m_s} are defined as the static power consumption of BS and RIS, respectively. The dynamic power consumption of BS and RIS are respectively defined by $\Delta_p P_{tr}$ and $Q P_{m_d}$, where $\frac{1}{\Delta_p}$ is the power amplifier efficiency and P_{m_d} is the average regulation power consumption per reflection element of RIS.

1) *Coverage probability*: The coverage probability $P_c(\delta)$ is defined as the probability of the typical UE's SINR γ_1 , which is greater than or equal to the threshold δ , expressed as

$$P_c(\delta) = 1 - P_o(\gamma_1 < \delta) = P(\gamma_1 \geq \delta), \quad (27)$$

where $P_o(\gamma_1 < \delta)$ represents the outage probability.

The power of the entire signal D_{sum} can be given as

$$|D_{sum}|^2 = |D_1 + D_2|^2 \approx \frac{|h_{1,1}|^2 P_{tr}}{(1 + d_{1,1}^D)^4} + \sum_{m=1}^M \frac{\beta_{1,m,1}^2 |h_{1,m,1}^C|^2 P_{tr}}{(1 + d_{m,1}^R)^4 (1 + d_{1,m}^I)^4} + \epsilon_1 + \epsilon_2, \quad (28)$$

where ϵ_1 and ϵ_2 are modified factors to simplify the analysis processing, and are respectively expressed as

$$\epsilon_1 = \sum_{m=1}^M \frac{\beta_{1,m,1} \sqrt{2\pi} \sigma_h |h_{1,m,1}^C| P_{tr}}{(1 + d_{1,1}^D)^2 (1 + d_{m,1}^R)^2 (1 + d_{1,m}^I)^2}, \quad (29a)$$

$$\epsilon_2 = \sum_{m=1}^M \sum_{\substack{m' \neq m \\ m'=1}}^M \frac{2\beta_{1,m,1} \beta_{1,m',1} |h_{1,m,1}^C| |h_{1,m',1}^C| P_{tr}}{(1 + d_{m,1}^R)^2 (1 + d_{1,m}^I)^2 (1 + d_{m',1}^R)^2 (1 + d_{1,m'}^I)^2}. \quad (29b)$$

In the RIS-assisted UDN system, the approximate closed formula for coverage probability can be deduced as

$$P(\gamma_1 \geq \delta) \approx \int_0^\infty \int_0^\infty \mathcal{W} \left(\mathcal{L}_{I_1} \mathcal{W} \left(\frac{\mathcal{L}_{I_2} \mathcal{L}_{D_2} \mathcal{L}_{\epsilon_1} \mathcal{W}(\mathcal{L}_{\epsilon_2}, \lambda_m)}{\int_0^\infty \mathcal{L}_{\epsilon_2} d_{m',1}^R dd_{m',1}^R}, \lambda_m \right), \lambda'_{un} \right) \exp \left(\frac{-(1 + d_{1,1}^D)^4 \delta \sigma_n^2}{2\sigma_h^2 P_{tr}} \right) f_{X_B}(x_b) dx_b f(d_{1,1}^D) dd_{1,1}^D, \quad (30)$$

where $\mathcal{W}(f(x), \lambda) \triangleq \exp(-2\pi\lambda \int (1 - f(x)) x dx)$, \mathcal{L}_x indicates the Laplace transform of the signal x , and the specific expressions and the proof are given in Appendix C.

When $\lambda_m = 0$, (30) can be degraded to a coverage expression for the UDN system without RIS. In addition, we found that there is a coverage limit for the UDN system, expressed as

$$P(\gamma_{udn} \geq \delta) \leq \int_0^\infty \exp \left(-2\pi\lambda'_{un} \int_{d_{1,1}^D}^\infty \left(1 - \frac{1}{1 + \frac{\delta(d_{1,1}^D)^4}{P_{tr}(d_{n,1}^D)^4}} \right) dd_{n,1}^D \right) f(d_{1,1}^D) dd_{1,1}^D = \frac{1}{1 + \sqrt{\delta} \arctan(\sqrt{\delta})}. \quad (31)$$

By deriving the partial derivative of (30) in Appendix C, it is found that the coverage probability is a monotonically decreasing function of λ'_{un} . This is understood that the interferences among BSs become larger and lead to smaller system coverage with the increase of λ'_{un} .

2) *Area Spectral Efficiency*: In general, ASE is widely used as an important performance metric for an UDN. The ASE is defined as the sum rate per bandwidth per area, expressed as

$$\eta_s = \frac{1}{\pi R^2} \sum_{n=1}^N \mathbb{E} [\log_2 (1 + \gamma_n)] = \lambda'_{un} \mathbb{E} [\log_2 (1 + \gamma)]. \quad (32)$$

In the RIS-assisted UDN, the approximate closed formula of ASE can be deduced as

$$\eta_s \approx \frac{\lambda'_{un}}{\ln 2} \int_0^\infty \int_0^\infty \int_0^\infty \frac{e^{-z\sigma_n^2}}{z} f(d_{1,1}^D) f_{X_B}(x_b) \left[\mathcal{W}(\mathcal{L}_{I_1}(z) \mathcal{W}(\mathcal{L}_{I_2}(z), \lambda_m), \lambda'_{un}) - \mathcal{L}_{D_1}(z) \mathcal{W}(\mathcal{L}_{I_1}(z) \mathcal{W}(\mathcal{L}_{I_2}(z) \mathcal{L}_{D_2}(z) \mathcal{L}_{\epsilon_1}(z) \mathcal{L}_{\epsilon_2}(z), \lambda_m), \lambda'_{un})) \right] dx_b dd_{1,1}^D dz \quad (33)$$

where the specific expressions and the proof are given in Appendix D.

In addition, the partial derivative analysis of ASE is also presented in Appendix D. It is found that the ASE is a monotonically increasing function of λ'_{un} , and there is a tendency to increase and then level off with the increase of λ'_{un} .

3) *Area Energy Efficiency*: The AEE is generally used to measure the energy consumption of a network, which is defined as the ratio of the ASE to the corresponding power consumption [16], [23], [29], expressed as

$$\eta_e = \frac{\eta_s}{\lambda'_{un}(\Delta_p P_{tr} + P_{n_s}) + \lambda_m(QP_{m_d} + P_{m_s})}, \quad (34)$$

where the unit scale of η_e is the bit /Joule/unit area.

4) *Energy Coverage Efficiency*: Since RIS can manipulate electromagnetic waves, it breaks the original way of radiation and coverage of the BS. To better analyze and describe the coverage reconfigurability of RIS-assisted system, energy coverage efficiency (ECE) is firstly defined in this paper, denoted as the ratio of the coverage probability to the corresponding power consumption with the unit scale of the coverage area per Watts, expressed as

$$\eta_c = \frac{\pi R^2 \mathbb{P}(\gamma_1 \geq \delta)}{N \bar{P}_n} = \frac{\mathbb{P}(\gamma_1 \geq \delta)}{\lambda'_{un} \bar{P}_n} = \frac{\mathbb{P}(\gamma_1 \geq \delta)}{\lambda'_{un}(\Delta_p P_{tr} + P_{n_s}) + \lambda_m(QP_{m_d} + P_{m_s})}, \quad (35)$$

where $\bar{P}_n = P_n + \frac{\lambda_m}{\lambda'_{un}} P_m$ is the normalization power consumption per BS.

V. SIMULATION RESULTS

This section simulates the performances of the proposed system in comparison with the classical UDN system. The power consumption of a BS refers to [30], and the RIS power consumption parameters are referred to [31]. We ignore the effect of the RIS reflection efficiency. For a fair comparison, the power amplifier efficiency of the BS is set to be ideal, i.e. $\Delta_p = 1$. The noise power is $\sigma_n^2 = N_0 B = 7.96 \times 10^{-14}$ W. Under the same RIS energy consumption, two parameter control groups are considered for comparing the effect of RIS deployment with

TABLE II: Simulation conditions.

System parameters	Values
Transmit power P_{tr}	30 dBm [30]
Static power consumption of BS P_{n_s}	14.7 W [30]
Power amplifier efficiency $\frac{1}{\Delta_p}$	1
Noise power spectral density N_0	-174 dBm/Hz
Bandwidth B	20 MHz
Path loss factor α	4
Small scale fading σ_h^2	$\sqrt{2}/2$
Radius of the given area R	1000 m
Intensity of active BS λ'_{un}	0.001 ~ 10 (m^{-2})
Intensity of RIS λ_m	0.005, 0.01, 0.05, 0.1 (m^{-2})
Number of reflection elements Q	10, 563
Dynamic power consumption of reflection element P_{m_d}	12 mW [31]
Static power consumption of RIS P_{m_s}	6.52 W [31]
Communication threshold δ	-30 ~ 50 dB

different parameters. One is $\lambda_m = 0.1, Q = 10$ and $\lambda_m = 0.05, Q = 563$, and the other is $\lambda_m = 0.01, Q = 10$ and $\lambda_m = 0.005, Q = 563$. The other simulation conditions are listed in Table II.

Fig. 5 shows the attribution probabilities and Poisson pair intensities of the RIS-assisted UDN system, where BS intensity is set to $\lambda_n = 0.01$. When $\frac{\lambda_u}{\lambda_n}$ increases, it can be seen that both the attribution probabilities and Poisson pair intensities increase. Since a larger $\frac{\lambda_u}{\lambda_n}$ means a greater active BS intensity λ'_{un} , the attribution probability of RIS becomes larger. Similarly, it can be found that the attribution probabilities and Poisson pair intensities have the same trend with $\frac{\lambda_m}{\lambda_n}$ increasing. For the attribution probability $P(u \neq 0)$ and Poisson pair intensity (Λ_N, Λ_U) , they can both be seen as the case of $\lambda_m \rightarrow \infty$. The case of $\lambda_m \rightarrow \infty$ is not achievable from the cost and energy efficiency perspective. Thus, there must exist a optimal case where the RIS intensity and the active BS intensity are matched. In addition, a larger $\frac{\lambda_m}{\lambda_n}$ brings the more obvious the effects when $\frac{\lambda_u}{\lambda_n}$ is larger. This indicates that the greater the active BS intensity, the greater the matching RIS intensity will be. The simulation curve is accord with the theoretical curve, verifying our previous analysis.

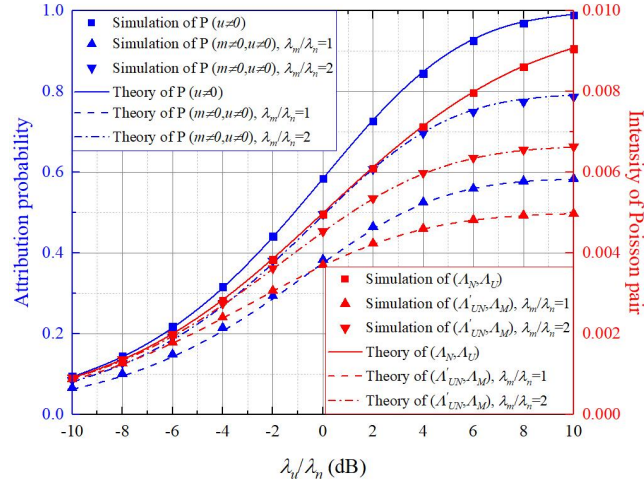


Fig. 5: The attribution probability and Poisson pair intensity of RIS-assisted UDN system with $\lambda_n = 0.01$.

Fig. 6 shows the average power of signals and interferences, where the RIS intensity are set to $\lambda_m = 0.1, 0.01$ and 0.005 , with the corresponding RIS reflection element number $Q = 10, 10$ and 563 . With the increase of active BS intensity λ'_{un} , the average power of signals are firstly rising and decreasing. This is because when the RIS intensity λ_m is a constant and the active BS intensity λ'_{un} increases, the area of each voronoi cell becomes smaller, indicating that the beamforming efficiency of RIS becomes smaller. Taking $\lambda_m = 0.005$ and $Q = 563$ as an example, it can be found that the average power of D_{sum} takes the maximum value when $\lambda'_{un} = 1$. On the left of the maximum value, we consider that it is the active BS intensity λ'_{un} limited area, while the right of the maximum value is the RIS intensity λ_m limited area. At the same RIS power consumption, a larger number of reflection elements can improve the average power of D_{sum} , since the higher number of reflection elements means the higher beamforming gain. For example, when $\lambda'_{un} = 0.1$, the case of $\lambda_m = 0.005, Q = 563$ is about 22 dB greater than the case of $\lambda_m = 0.01, Q = 10$.

Fig. 7 shows that the outage probabilities of the typical UE, where the active BS intensity is set to $\lambda'_{un} = 0.01$. In general, the UDN system with RIS can improve the typical UE's outage probability compared with the classical UDN system. There is an interesting phenomenon, under a low communication threshold δ , the UDN system with RIS is even worse than the classical UDN system, since the RIS simultaneously improves both the signals and interferences of the cell edge UEs (low SINR UEs). We call this phenomenon which upgrades the high SINR UEs and downgrades the low SINR UEs as the Matthew's effect of RIS-assisted UDN system. With

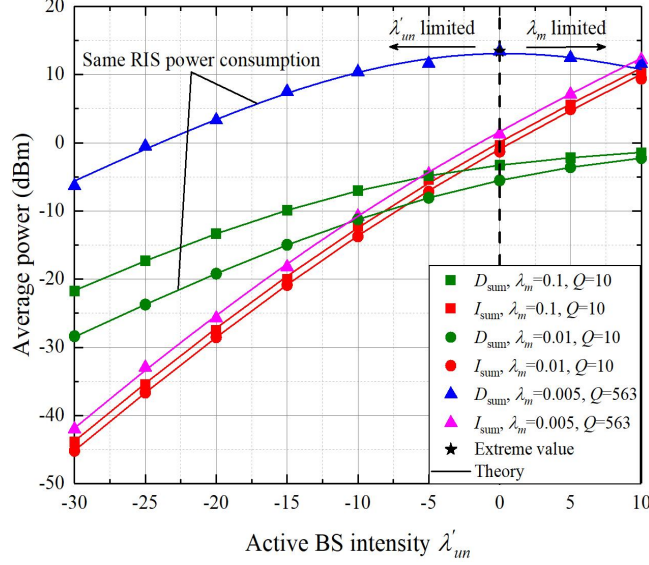


Fig. 6: The average power of signals and interferences in the case of $\lambda_m = 0.1, 0.01$ and 0.005 .

the same RIS power consumption, it can be found that the case of $\lambda_m = 0.05, Q = 563$ provides good assistance to cell center UEs (high SINR UEs), and the case of $\lambda_m = 0.01, Q = 10$ provides good assistance to cell edge UEs (low SINR UEs). For example, when $\gamma_1 = 30$ dB, the outage probability of $\lambda_m = 0.05, Q = 563$ is about 77% of the case of $\lambda_m = 0.01, Q = 10$. And when $\gamma_1 = -20$ dB, the outage probability of $\lambda_m = 0.05, Q = 563$ is about 3.6 times larger than the case of $\lambda_m = 0.01, Q = 10$. since a large number of reflection elements can greatly enhance the signals of cell center UEs (high SINR UEs).

The coverage probabilities of the RIS-assisted UDN and classical UDN are shown in Fig. 8, where $\lambda_m = 0.1, 0.01, 0.05, 0.005$ and $Q = 10, 10, 563, 563$. With the increased active BS intensity λ'_{un} , the coverage probability shows a decreasing trend, because of the increased interferences from other BSs. In general, the RIS-assisted UDN system can provide much better coverage probability than the case without RIS. For example, when $\lambda'_{un} = 0.001$, the coverage probability of the case of $\lambda_m = 0.05, Q = 563$ is improved about 48% than the case without RIS. Besides, it is found that a larger number of reflection elements is more sensitive to the active BS intensity λ'_{un} , since a larger number of reflection elements may bring more interferences. For example, when $\lambda'_{un} = 0.001$, the case of $\lambda_m = 0.05, Q = 563$ is about 4% better than the case of $\lambda_m = 0.1, Q = 10$, and when $\lambda_m = 0.1$, the case of $\lambda_m = 0.05, Q = 563$ is about 18% worse than the case of $\lambda_m = 0.1, Q = 10$. In addition, the simulation curve is accord with the

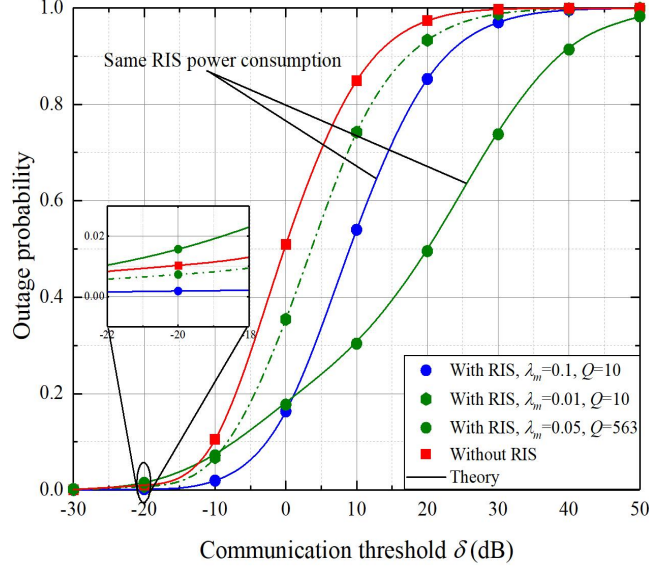


Fig. 7: The outage probability of the typical UE with $\lambda'_{un} = 0.01$.

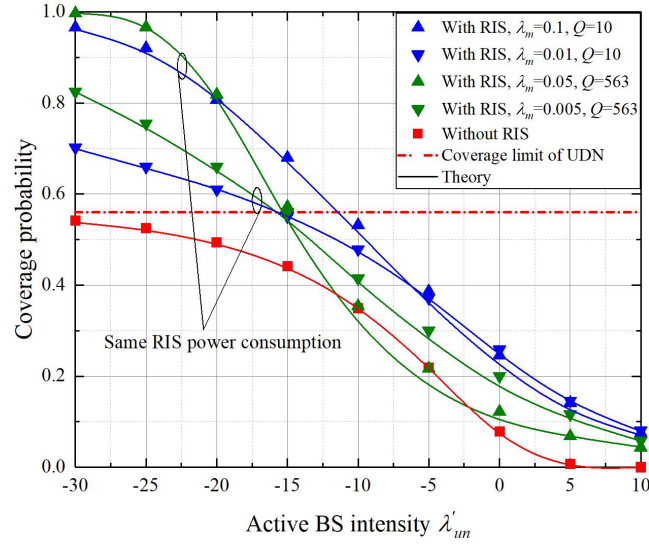


Fig. 8: The coverage probability of RIS-assisted UDN system, where $\lambda_m = 0.1, 0.01, 0.05$ and 0.005 .

theoretical curve.

Fig. 9 shows the ASE performances of the RIS-assisted UDN and the classical UDN systems, where $\lambda_m = 0.1, 0.01, 0.05$ and 0.005 . Compared to the classical UDN system, the RIS-assisted UDN system can provide higher ASE. For example, when $\lambda'_{un} = 0.001$, $\lambda_m = 0.05$ and $Q = 563$, the RIS-assisted UDN system is about 402% higher than the classical UDN system. With the same RIS power consumption, the RIS-assisted effect of ASE is similar to that of the coverage

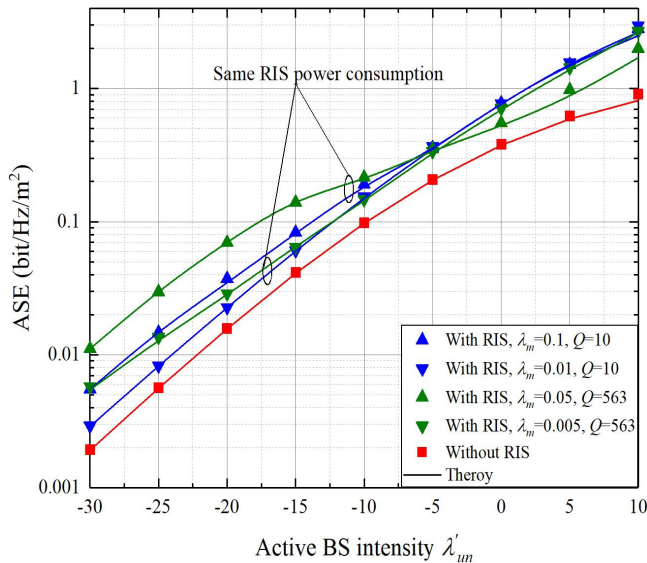


Fig. 9: The ASE of RIS-assisted UDN system with $\lambda_m = 0.1, 0.01, 0.05$ and 0.005 .

probability. Therefore, there is the performance inversion when the active BS intensity λ'_{un} is larger. For example, when $\lambda'_{un} = 0.001$, the case of $\lambda_m = 0.05, Q = 563$ is about 267% better than the case of $\lambda_m = 0.1, Q = 10$. When $\lambda'_{un} = 10$, the case of $\lambda_m = 0.05, Q = 563$ is about 63% worse than the case of $\lambda_m = 0.1, Q = 10$. The simulated results are also accord with the theoretical results.

The AEE performances of RIS-assisted UDN system and the classical UDN system are shown in Fig. 10, where $\lambda_m = 0.1, 0.01, 0.05$ and 0.005 . For a given active BS intensity λ'_{un} , it is always possible to find a RIS scheme that makes the RIS-assisted UDN system superior to the classical UDN system. With the increase of active BS intensity λ'_{un} , it is found that the AEE performance of the RIS-assisted UDN system has an extreme value in the RIS-assisted UDN system, since the major energy consumption is from RISs which is a linear increased function. When λ'_{un} is larger, the energy consumption is mainly from the BSs; on the contrary, it comes mainly from the RISs. Taking $\lambda_m = 0.1, Q = 10$ as an example, When $\lambda'_{un} = 0.1$, the AEE performance of the case of $\lambda_m = 0.1, Q = 10$ is about 33% better than the classical UDN system. When $\lambda'_{un} = 0.01$, the RIS-assisted UDN system is about 122% worse than the classical UDN system. Therefore, the configuration of RIS should be matched an optimal active BS intensity, to balance the energy consumption and spectral efficiency.

The ECE performance of the RIS-assisted UDN system and classical UND systems are shown

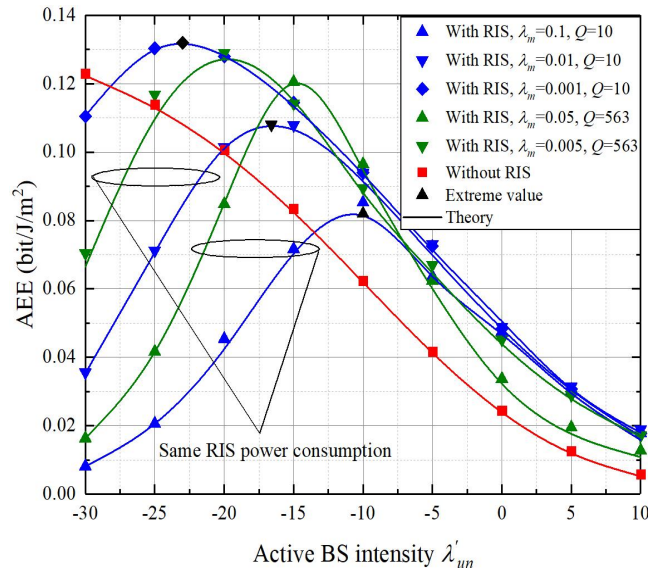


Fig. 10: The AEE of RIS-assisted UDN system with $\lambda_m = 0.1, 0.01, 0.05$ and 0.005 .

in Fig. 11, where $\lambda_m = 0.1, 0.01, 0.05$ and 0.005 . Overall, the ECE decreases as the intensity of active BSs λ'_{un} increases, since the reduction of the BS coverage area caused by the interferences of the dense network. Moreover, the ECE of the system with RIS is more robust than that of the classical UDN system. For example, the classical UDN system changes by about 22.1 dB from $\lambda'_{un} = 0.01$ to $\lambda'_{un} = 3.16$, while the RIS system with $\lambda_m = 0.1, Q = 10$ only changes by about 12.7 dB. This is because the RIS can enhance the signal effect to slow down the reduction of coverage area.

VI. CONCLUSION

This paper proposes the ternary stochastic geometry theory for analyzing the RIS-assisted UDN system. We first define the typical \triangle BRU as the basic unit of the ternary network, which can help analyze the interrelationships of multiple point processes. Based on the geometric relationships of the typical \triangle BRU, we analyze the attribution probability and deduce the PDFs of the correlation edges and angles. Furthermore, we present the ternary Campbell's theorem and the ternary PGFL analysis to calculate the random sum and random product of ternary systems. Then, we comprehensively analyze the system performances, including the coverage probability, ASE, AEE and ECE. Simulation results show that the RIS-assisted UDN system generally outperforms the classical UDN system in all performance aspects. The random deployment of RIS leads to the Matthew effect, i.e., RISs can improve the SINR of cell center UEs, while weakening

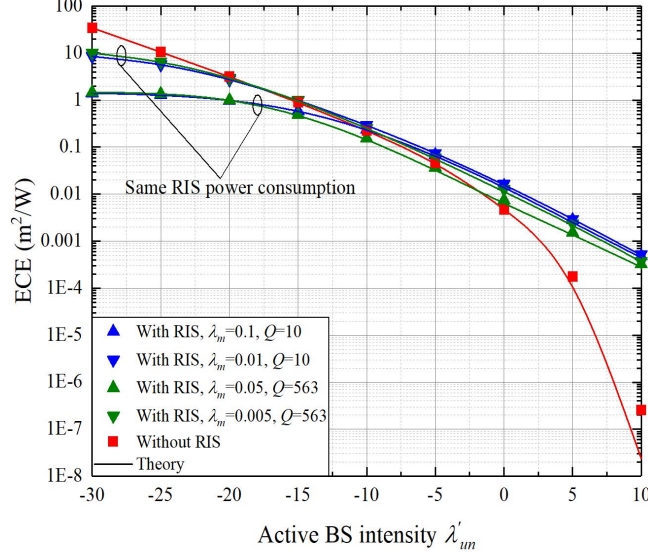


Fig. 11: The ECE of the RIS-assisted UDN system with $\lambda_m = 0.1, 0.01, 0.05$ and 0.005 .

the SINR of cell edge UEs. Moreover, for the same RIS power consumption, the deployment scheme with higher RIS intensity is more suitable for denser UDN systems, while the deployment scheme with larger number of RIS reflection elements is more suitable for sparser UDN systems. This leads us to explore the specific relationship between communication requirements and RIS configurations in future research. It is important to consider the effect of environment, e.g., building, tree, vehicle, and ect., which may bring in new challenges.

APPENDIX A

Recall Section II, the average power of D_1 can be expressed as

$$\mathbb{E} \left[|D_1|^2 \right] \stackrel{(a)}{=} P_{tr} \cdot \mathbb{E} [|h_{1,1}|^2] \cdot \mathbb{E} \left[(1 + d_{1,1}^D)^{-4} \right] = 4\pi \lambda'_{un} P_{tr} \sigma_h^2 \mathcal{F}(4, \pi \lambda'_{un}), \quad (36)$$

where (a) is due to the independence of the random variables.

Next, the reflected signals D_2 is further given as

$$D_2 = \sum_{m \in \Psi^M} \frac{h_{1,m,1} \beta_{1,m,1} s_1}{(1 + d_{m,1}^R)^2 (1 + d_{1,m}^I)^2} = \underbrace{\sum_{m \in \Psi_1^M} \frac{h_{1,m,1} \beta_{1,m,1} s_1}{(1 + d_{m,1}^R)^2 (1 + d_{1,m}^I)^2}}_{D_{2,\Psi_1^M}} + \underbrace{\sum_{m \in \tilde{\Psi}_1^M} \frac{h_{1,m,1} \beta_{1,m,1} s_1}{(1 + d_{m,1}^R)^2 (1 + d_{1,m}^I)^2}}_{D_{2,\tilde{\Psi}_1^M}}, \quad (37)$$

where D_{2,Ψ_1^M} and $D_{2,\tilde{\Psi}_1^M}$ respectively represent the reflected signals of the RISs belonging to the typical BS, and the rest RISs.

As aforementioned, the expectation of D_{2,Ψ_1^M} and $D_{2,\tilde{\Psi}_1^M}$ conditional on x_b and $d_{1,1}^D$ are respectively expressed as

$$\begin{aligned} \mathbb{E}\left[|D_{2,\Psi_1^M}|^2|x_b, d_{1,1}^D\right] &\stackrel{(a)}{=} \left(4 - \frac{\pi^2}{4} + \frac{\pi^2}{4}Q\right) Q\sigma_h^4 P_{tr} \cdot 2\pi\lambda_m \int_0^{\sqrt{\frac{x_b}{\pi\lambda_{un}}}} \mathcal{Q}\left(\frac{1}{(1+d_{m,1}^R)^4(1+d_{1,m}^I)^4}\right) d_{1,m}^I \mathbb{d}d_{1,m}^I \\ &\quad + \frac{\pi^2}{4}Q^2\sigma_h^4 P_{tr} \left(2\pi\lambda_m \int_0^{\sqrt{\frac{x_b}{\pi\lambda_{un}}}} \mathcal{Q}\left(\frac{1}{(1+d_{m,1}^R)^2(1+d_{1,m}^I)^2}\right) d_{1,m}^I \mathbb{d}d_{1,m}^I\right)^2, \end{aligned} \quad (38a)$$

$$\mathbb{E}\left[|D_{2,\tilde{\Psi}_1^M}|^2|x_b, d_{1,1}^D\right] \stackrel{(a)}{=} 8\pi\lambda_m Q\sigma_h^4 P_{tr} \int_0^{\sqrt{\frac{x_b}{\pi\lambda_{un}}}} \mathcal{Q}\left(\frac{1}{(1+d_{m,1}^R)^4(1+d_{1,m}^I)^4}\right) d_{1,m}^I \mathbb{d}d_{1,m}^I, \quad (38b)$$

where (a) follows the Ternary Campbell's theorem.

Finally, we deduce the average power of the entire signal D_{sum} , expressed as

$$\begin{aligned} \mathbb{E}\left[|D_{sum}|^2\right] &= P_{tr} \int_0^\infty \int_0^\infty \left\{ \mathbb{E}\left[|D_1 + D_{2,\Psi_1^M}|^2 + |D_{2,\tilde{\Psi}_1^M}|^2|x_b, d_{1,1}^D\right] \right\} f_{X_B}(x_b) dx_b f(d_{1,1}^D) \mathbb{d}d_{1,1}^D \\ &= P_{tr} \int_0^\infty \int_0^\infty \left\{ \left[\frac{\pi^3}{2} (Q-1) Q\sigma_h^4 \lambda_m \int_0^{\sqrt{\frac{x_b}{\pi\lambda_{un}}}} \mathcal{Q}\left(\frac{1}{(1+d_{m,1}^R)^4(1+d_{1,m}^I)^4}\right) d_{1,m}^I \mathbb{d}d_{1,m}^I \right. \right. \\ &\quad \left. \left. + \pi^4 Q^2 \sigma_h^4 \lambda_m^2 \left(\int_0^{\sqrt{\frac{x_b}{\pi\lambda_{un}}}} \mathcal{Q}\left(\frac{1}{(1+d_{m,1}^R)^2(1+d_{1,m}^I)^2}\right) d_{1,m}^I \mathbb{d}d_{1,m}^I \right)^2 + \frac{2\sigma_h^2}{(1+d_{1,1}^D)^4} \right. \right. \\ &\quad \left. \left. + \frac{\sqrt{2\pi^5} Q\sigma_h^3 \lambda_m}{(1+d_{1,1}^D)^2} \int_0^{\sqrt{\frac{x_b}{\pi\lambda_{un}}}} \mathcal{Q}\left(\frac{1}{(1+d_{m,1}^R)^2(1+d_{1,m}^I)^2}\right) d_{1,m}^I \mathbb{d}d_{1,m}^I \right] f_{X_B}(x_b) dx_b \right. \\ &\quad \left. + 8\pi\lambda_m Q\sigma_h^4 \int_0^\infty \mathcal{Q}\left(\frac{1}{(1+d_{m,1}^R)^4(1+d_{1,m}^I)^4}\right) d_{1,m}^I \mathbb{d}d_{1,m}^I \right\} f(d_{1,1}^D) \mathbb{d}d_{1,1}^D. \end{aligned} \quad (39)$$

APPENDIX B

Recall Section II, the average power of interferences I_1 and I_2 are respectively expressed as

$$\mathbb{E}\left[|I_1|^2\right] \stackrel{(a)}{=} 2P_{tr}\sigma_h^2 \int_0^\infty \int_{d_{1,1}^D}^\infty 2\pi\lambda_{un} x(1+x)^{-4} dx f(d_{1,1}^D) \mathbb{d}d_{1,1}^D = 4\pi P_{tr}\sigma_h^2 \lambda_{un} \left[\frac{1}{6} - \mathcal{F}(4, \pi\lambda_{un}') \right], \quad (40a)$$

$$\begin{aligned} \mathbb{E}\left[|I_2|^2\right] &\stackrel{(a)}{=} 4Q\sigma_h^4 P_{tr} \mathbb{E}\left[\sum_{n' \neq n, n'=1}^N (1+d_{n',m}^I)^{-4} 2\lambda_m \pi \int_0^\infty \mathcal{Q}\left(\frac{1}{(1+d_{m,1}^R)^4}\right) d_{m,1}^R \mathbb{d}d_{m,1}^R \right] \\ &= 16\pi^2 Q\sigma_h^4 P_{tr} \lambda_m \lambda_{un}' \iiint \mathcal{Q}\left(\frac{1}{(1+d_{m,1}^R)^4(1+d_{n',m}^I)^4}\right) d_{m,1}^R \mathbb{d}d_{m,1}^R d_{n',1}^D \mathbb{d}d_{n',1}^D f(d_{1,1}^D) \mathbb{d}d_{1,1}^D, \end{aligned} \quad (40b)$$

where (a) and (b) both follow the Campbell's theorem.

Thereafter, the average power of the entire interference I_{sum} is deduced as

$$\begin{aligned} \mathbb{E}\left[|I_{sum}|^2\right] &= \mathbb{E}\left[|I_1|^2\right] + \mathbb{E}\left[|I_2|^2\right] = 4\pi P_{tr}\sigma_h^2 \lambda_{un}' \left[4Q\pi\lambda_m \sigma_h^2 \int_0^\infty \int_{d_{1,1}^D}^\infty \int_0^\infty \mathcal{Q}\left(\frac{1}{(1+d_{m,1}^R)^4(1+d_{n',m}^I)^4}\right) \right. \\ &\quad \left. d_{m,1}^R \mathbb{d}d_{m,1}^R d_{n',1}^D \mathbb{d}d_{n',1}^D f(d_{1,1}^D) \mathbb{d}d_{1,1}^D + \frac{1}{6} - \mathcal{F}(4, \pi\lambda_{un}') \right]. \end{aligned} \quad (41)$$

APPENDIX C

For mathematic convenience, the small-scale channel fading gains are transformed by Laplace transform as

$$\mathcal{L}_{D_1}(s) = \text{E} [\exp(-s|h_{1,1}|^2)] = \frac{1}{1 + 2\sigma_h^2 s}, \quad (42a)$$

$$\mathcal{L}_{D_2}(s) = \text{E} [\exp(-s|h_{1,m,1}|^2)] = \begin{cases} \frac{\exp\left(-\frac{Q^2\sigma_h^4\pi^2 s}{4+(32-2\pi^2)Q\sigma_h^4 s}\right)}{\sqrt{1+(8-\frac{\pi^2}{2})Q\sigma_h^4 s}}, & m \in \Psi_1^M, \\ \frac{1}{1+4Q\sigma_h^4 s}, & m \notin \Psi_1^M, \end{cases} \quad (42b)$$

$$\mathcal{L}_{I_1}(s) = \text{E} [\exp(-s|h_{n',1}|^2)] = \frac{1}{1 + 2\sigma_h^2 s}, \quad (42c)$$

$$\mathcal{L}_{I_2}(s) = \text{E} [\exp(-s|h_{n',m,1}|^2)] = \frac{1}{1 + 4Q\sigma_h^4 s}, \quad (42d)$$

$$\mathcal{L}_{\epsilon_1}(s) = \text{E} [\exp(-s|h_{1,m,1}|)] = \begin{cases} \exp\left(\left(2 - \frac{\pi^2}{8}\right)Q\sigma_h^4 s^2 + \frac{\pi}{2}Q\sigma_h^2 s\right), & m \in \Psi_1^M, \\ \exp\left(\left(2 - \frac{\pi^2}{8}\right)Q\sigma_h^4 s^2\right), & m \notin \Psi_1^M, \end{cases} \quad (42e)$$

$$\mathcal{L}_{\epsilon_2}(s) = \text{E} [\exp(-s|h_{1,m,1}||h_{1,m',1}|)] = \begin{cases} \frac{\exp\left(-\frac{\pi^2 Q^2 \sigma_h^4 s}{4+(16-\pi^2)Q\sigma_h^4 s}\right)}{\sqrt{1-(4-\frac{\pi^2}{4})^2 Q^2 \sigma_h^8 s^2}}, & m, m' \in \Psi_1^M, \\ \leq \frac{1}{1-(4-\frac{\pi^2}{4})^2 Q^2 \sigma_h^8 s^2}, & \text{others.} \end{cases} \quad (42f)$$

Thus, the coverage probability of the RIS-assisted UDN system is

$$\begin{aligned} & \text{P}(\gamma_1 \geq \delta) \\ & \stackrel{(a)}{\approx} \text{E} \left[\exp\left(-\frac{(1+d_{1,1}^D)^4}{2\sigma_h^2 P_{tr}} \left[\delta \left(\sum_{n'=2}^N \frac{|h_{n',u}|^2 P_{tr}}{(1+d_{n',u}^D)^4} + \sum_{n'=2}^N \sum_{m=1}^M \frac{\beta_{n',m,1}^2 |h_{n',m,1}^C|^2 P_{tr}}{(1+d_{n',m}^I)^4 (1+d_{m,1}^R)^4} + \sigma_n^2 \right) \right. \right. \right. \\ & \quad \left. \left. \left. - \sum_{m=1}^M \frac{\beta_{1,m,1}^2 |h_{1,m,1}^C|^2 P_{tr}}{(1+d_{m,1}^R)^4 (1+d_{1,m}^I)^4} - \epsilon_1 - \epsilon_2 \right) \right] \right) \\ & = \text{E} \left[\exp\left(-\frac{(1+d_{1,1}^D)^4 \delta \sigma_n^2}{2\sigma_h^2 P_{tr}}\right) \prod_{m=1}^M \mathcal{L}_{\epsilon_1} \left(-\frac{\sqrt{2\pi} \beta_{1,m,1} (1+d_{1,1}^D)^2}{2\sigma_h (1+d_{m,1}^R)^2 (1+d_{1,m}^I)^2} \right) \prod_{n'=2}^N \mathcal{L}_{I_1} \left(\frac{(1+d_{1,1}^D)^4 \delta}{2\sigma_h^2 (1+d_{n',u}^D)^4} \right) \right. \\ & \quad \prod_{n'=2}^N \prod_{m=1}^M \mathcal{L}_{I_2} \left(\frac{\beta_{n',m,1}^2 (1+d_{1,1}^D)^4 \delta}{2\sigma_h^2 (1+d_{n',m}^I)^4 (1+d_{m,1}^R)^4} \right) \prod_{m=1}^M \mathcal{L}_{D_2} \left(-\frac{\beta_{1,m,1}^2 (1+d_{1,1}^D)^4 \delta}{2\sigma_h^2 (1+d_{m,1}^R)^4 (1+d_{1,m}^I)^4} \right) \\ & \quad \left. \prod_{m=1}^M \prod_{\substack{m' \neq m, \\ m'=1}}^M \mathcal{L}_{\epsilon_2} \left(-\frac{(1+d_{1,1}^D)^4 \beta_{1,m,1} \beta_{1,m',1}}{2\sigma_h^2 (1+d_{m,1}^R)^2 (1+d_{1,m}^I)^2 (1+d_{m',1}^R)^2 (1+d_{1,m'}^I)^2} \right) \right] \\ & \approx \text{E} \left[\exp\left(-\frac{(1+d_{1,1}^D)^4 \delta \sigma_n^2}{2\sigma_h^2 P_{tr}}\right) \prod_{n'=2}^N \mathcal{L}_{I_1} \prod_{m=1}^M \mathcal{L}_{I_2} \mathcal{L}_{D_2} \mathcal{L}_{\epsilon_1} \frac{\exp(-2\pi\lambda_m \int_0^\infty (1-\mathcal{L}_{\epsilon_2}) d_{m',1}^R dd_{m',1}^R)}{\int_0^\infty \mathcal{L}_{\epsilon_2} d_{m',1}^R dd_{m',1}^R} \right] \\ & = \int_0^\infty \int_0^\infty \mathcal{W} \left(\mathcal{L}_{I_1} \mathcal{W} \left(\frac{\mathcal{L}_{I_2} \mathcal{L}_{D_2} \mathcal{L}_{\epsilon_1} \mathcal{W}(\mathcal{L}_{\epsilon_2}, \lambda_m)}{\int_0^\infty \mathcal{L}_{\epsilon_2} d_{m',1}^R dd_{m',1}^R}, \lambda_m \right), \lambda_{un} \right) \exp\left(-\frac{(1+d_{1,1}^D)^4 \delta \sigma_n^2}{2\sigma_h^2 P_{tr}}\right) f_{X_B}(x_b) dx_b f(d_{1,1}^D) dd_{1,1}^D, \end{aligned} \quad (43)$$

where (a) follows $|h_{1,1}|^2 \sim \exp\left(\frac{1}{2\sigma_h^2}\right)$, and $\mathcal{W}(f(x), \lambda) \triangleq \exp\left(-2\pi\lambda \int (1-f(x))x dx\right)$.

Furthermore, the partial derivative of coverage probability with respect to the active BS intensity λ'_{un} can be expressed as

$$\begin{aligned} \frac{\partial \mathcal{P}(\gamma_1 \geq \delta)}{\partial \lambda'_{un}} &\xrightarrow{\text{approx}} \frac{\partial \int_0^\infty \mathcal{W}(x, \lambda'_{un}) 2\pi \lambda'_{un} x \exp(-\pi \lambda'_{un} x^2) dx}{\partial \lambda'_{un}} \\ &\xrightarrow{(a)} \int_0^\infty \left[2\pi \lambda'_{un} - 4\pi^2 \lambda'_{un} x^2 - 4\pi^2 \lambda'_{un} x \int (1-f(y))y dy \right] dx \leq 0, \end{aligned} \quad (44)$$

where (a) is to remove the positive term from the integral.

APPENDIX D

The ASE is defined as the sum rate per bandwidth per area, as

$$\eta_s = \frac{1}{\pi R^2} \sum_{n=1}^N \mathbb{E}[\log_2(1 + \gamma_n)] = \lambda'_{un} \mathbb{E}[\log_2(1 + \gamma)] = \frac{\lambda'_{un}}{\ln 2} \int_0^\infty [\mathcal{M}_I(z) - \mathcal{M}_{I+D}(z)] \frac{e^{-z\sigma_n^2}}{z} dz, \quad (45)$$

where $\mathcal{M}_x(z) = \mathbb{E}[e^{-zx}]$ is the moment generation function (MGF) of x . According to Lemma 2, $\mathcal{M}_I(z)$ and $\mathcal{M}_{I+D}(z)$ are given as

$$\begin{aligned} \mathcal{M}_I(z) &= \mathbb{E} \left[\exp \left(-z \left(\sum_{n'=2}^N \frac{|h_{n',u}|^2 P_{tr}}{(1+d_{n',u}^D)^4} + \sum_{n'=2m=1}^M \frac{\beta_{n',m,1}^2 |h_{n',m,1}^C|^2 P_{tr}}{(1+d_{n',m}^I)^4 (1+d_{m,1}^R)^4} \right) \right) \right] \\ &= \mathbb{E} \left[\prod_{n'=2}^N \mathcal{L}_{I_1} \left(\frac{z P_{tr}}{(1+d_{n',u}^D)^4} \right) \prod_{n'=2}^N \prod_{m=1}^M \mathcal{L}_{I_2} \left(\frac{z P_{tr} \beta_{n',m,1}^2}{(1+d_{n',m}^I)^4 (1+d_{m,1}^R)^4} \right) \right] \\ &= \int_0^\infty \int_0^\infty \mathcal{W}(\mathcal{L}_{I_1}(z) \mathcal{W}(\mathcal{L}_{I_2}(z), \lambda_m), \lambda'_{un}) f_{X_B}(x_b) dx_b f(d_{1,1}^D) dd_{1,1}^D, \end{aligned} \quad (46a)$$

$$\begin{aligned} \mathcal{M}_{I+D}(z) &= \mathbb{E} \left[\exp \left(-z \left(\sum_{n'=2}^N \frac{|h_{n',u}|^2 P_{tr}}{(1+d_{n',u}^D)^4} + \sum_{n'=2m=1}^M \frac{\beta_{n',m,1}^2 |h_{n',m,1}^C|^2 P_{tr}}{(1+d_{n',m}^I)^4 (1+d_{m,1}^R)^4} + |D_1 + D_2|^2 \right) \right) \right] \\ &\approx \mathbb{E} \left[\exp \left(-z \left(\sum_{n'=2}^N \frac{|h_{n',u}|^2 P_{tr}}{(1+d_{n',u}^D)^4} + \sum_{n'=2}^N \sum_{m=1}^M \frac{\beta_{n',m,1}^2 |h_{n',m,1}^C|^2 P_{tr}}{(1+d_{n',m}^I)^4 (1+d_{m,1}^R)^4} + \frac{|h_{1,1}|^2 P_{tr}}{(1+d_{1,1}^D)^4} \right. \right. \\ &\quad \left. \left. + \sum_{m=1}^M \frac{\beta_{1,m,1}^2 |h_{1,m,1}^C|^2 P_{tr}}{(1+d_{m,1}^R)^4 (1+d_{1,m}^I)^4} + \epsilon_1 + \epsilon_2 \right) \right) \right] \\ &= \mathbb{E} \left[\mathcal{L}_{D_1}(z) \prod_{n'=2}^N \mathcal{L}_{I_1}(z) \prod_{n'=2}^N \prod_{m=1}^M \mathcal{L}_{I_2}(z) \mathcal{L}_{D_2}(z) \mathcal{L}_{\epsilon_1}(z) \frac{\mathcal{W}(\mathcal{L}_{\epsilon_2}(z), \lambda_m)}{\int_0^\infty \mathcal{L}_{\epsilon_2} d_{m',1}^R dd_{m',1}^R} \right] \\ &= \int_0^\infty \int_0^\infty \mathcal{L}_{D_1}(z) \mathcal{W}(\mathcal{L}_{I_1}(z) \mathcal{W}(\frac{\mathcal{L}_{I_2}(z) \mathcal{L}_{D_2}(z) \mathcal{L}_{\epsilon_1}(z) \mathcal{W}(\mathcal{L}_{\epsilon_2}(z), \lambda_m)}{\int_0^\infty \mathcal{L}_{\epsilon_2} d_{m',1}^R dd_{m',1}^R}, \lambda_m), \lambda'_{un}) f_{X_B}(x_b) dx_b f(d_{1,1}^D) dd_{1,1}^D. \end{aligned} \quad (46b)$$

Thus, the ASE of the RIS-assisted system is shown in (33). The partial derivative of ASE with respect to the active BS intensity λ'_{un} can be expressed as

$$\frac{\partial \eta_s}{\partial \lambda'_{un}} \xrightarrow{\text{approx}} \mathbb{E}[\log_2(1 + \gamma_1)] \geq 0, \quad (47)$$

where it can be seen from the statistical properties of the received signals that $\mathbb{E}[\log_2(1 + \gamma_1)]$ converges to 0 when $\lambda'_{un} \rightarrow 0$. Therefore, the ASE should generally show an increasing and gradually leveling off trend.

REFERENCES

- [1] Q. Wu and R. Zhang, "Towards Smart and Reconfigurable Environment: Intelligent Reflecting Surface Aided Wireless Network," *IEEE Communications Magazine*, vol. 58, no. 1, pp. 106-112, January 2020.
- [2] H. ElSawy, A. Sultan-Salem, M. -S. Alouini and M. Z. Win, "Modeling and Analysis of Cellular Networks Using Stochastic Geometry: A Tutorial," *IEEE Communications Surveys & Tutorials*, vol. 19, no. 1, pp. 167-203, Firstquarter 2017.
- [3] H. ElSawy, E. Hossain and M. Haenggi, "Stochastic Geometry for Modeling, Analysis, and Design of Multi-Tier and Cognitive Cellular Wireless Networks: A Survey," *IEEE Communications Surveys & Tutorials*, vol. 15, no. 3, pp. 996-1019, Third Quarter 2013.
- [4] Y. Deng, L. Wang, M. Elkashlan, A. Nallanathan and R. K. Mallik, "Physical Layer Security in Three-Tier Wireless Sensor Networks: A Stochastic Geometry Approach," *IEEE Transactions on Information Forensics and Security*, vol. 11, no. 6, pp. 1128-1138, June 2016.
- [5] W. Yi, Y. Liu and A. Nallanathan, "Cache-Enabled HetNets With Millimeter Wave Small Cells," *IEEE Transactions on Communications*, vol. 66, no. 11, pp. 5497-5511, Nov. 2018.
- [6] H. S. Dhillon, R. K. Ganti, F. Baccelli and J. G. Andrews, "Modeling and Analysis of K-Tier Downlink Heterogeneous Cellular Networks," *IEEE Journal on Selected Areas in Communications*, vol. 30, no. 3, pp. 550-560, April 2012.
- [7] W. Wen, Y. Cui, F. -C. Zheng, S. Jin and Y. Jiang, "Enhancing Performance of Random Caching in Large-Scale Heterogeneous Wireless Networks With Random Discontinuous Transmission," *IEEE Transactions on Communications*, vol. 66, no. 12, pp. 6287-6303, Dec. 2018.
- [8] W. Yi, Y. Liu, Y. Deng and A. Nallanathan, "Clustered UAV Networks With Millimeter Wave Communications: A Stochastic Geometry View," *IEEE Transactions on Communications*, vol. 68, no. 7, pp. 4342-4357, July 2020.
- [9] W. Lu and M. Di Renzo, "Stochastic Geometry Modeling and System-Level Analysis & Optimization of Relay-Aided Downlink Cellular Networks," *IEEE Transactions on Communications*, vol. 63, no. 11, pp. 4063-4085, Nov. 2015.
- [10] Z. Gu, H. Lu, M. Zhang, H. Sun and C. W. Chen, "Association and Caching in Relay-Assisted mmWave Networks: A Stochastic Geometry Perspective," *IEEE Transactions on Wireless Communications*, vol. 20, no. 12, pp. 8316-8332, Dec. 2021.
- [11] A. Al-Hourani, S. Kandeepan and A. Jamalipour, "Stochastic Geometry Study on Device-to-Device Communication as a Disaster Relief Solution," *IEEE Transactions on Vehicular Technology*, vol. 65, no. 5, pp. 3005-3017, May 2016.
- [12] M. Ragheb, S. M. S. Hemami, A. Kuhestani, D. W. K. Ng and L. Hanzo, "On the Physical Layer Security of Untrusted Millimeter Wave Relaying Networks: A Stochastic Geometry Approach," *IEEE Transactions on Information Forensics and Security*, vol. 17, pp. 53-68, 2022.
- [13] Bagherinejad S, Bayanifar M, Maleki M S, et al, "Coverage probability of RIS-assisted mmWave cellular networks under blockages: A stochastic geometric approach," *Physical Communication*, vol. 53, pp. 101740, Aug. 2022.
- [14] T. Shafique, H. Tabassum and E. Hossain, "Stochastic Geometry Analysis of IRS-Assisted Downlink Cellular Networks," *IEEE Transactions on Communications*, vol. 70, no. 2, pp. 1442-1456, Feb. 2022.
- [15] C. Psomas, H. A. Suraweera and I. Krikidis, "On the Association with Intelligent Reflecting Surfaces in Spatially Random Networks," *ICC 2021 - IEEE International Conference on Communications*, pp. 1-6, 2021.
- [16] Y. Xu, S. Zhou and Z. Niu, "The Impact of Interference Reflection on Reconfigurable Intelligent Surface-Aided Directional Transmissions," *2021 IEEE/CIC International Conference on Communications in China (ICCC)*, pp. 207-212, 2021.
- [17] M. A. Kishk and M. -S. Alouini, "Exploiting Randomly Located Blockages for Large-Scale Deployment of Intelligent Surfaces," *IEEE Journal on Selected Areas in Communications*, vol. 39, no. 4, pp. 1043-1056, April 2021.

- [18] M. Nemati, J. Park and J. Choi, "RIS-assisted Coverage Enhancement in Millimeter-Wave Cellular Networks," *IEEE Access*, vol. 8, pp. 188171-188185, 2020.
- [19] J. Lyu and R. Zhang, "Spatial Throughput Characterization for Intelligent Reflecting Surface Aided Multiuser System," *IEEE Wireless Communications Letters*, vol. 9, no. 6, pp. 834-838, June 2020.
- [20] J. Lyu and R. Zhang, "Hybrid Active/Passive Wireless Network Aided by Intelligent Reflecting Surface: System Modeling and Performance Analysis," *IEEE Transactions on Wireless Communications*.
- [21] Li Y, Chun Y J, "Stochastic Geometric Analysis of IRS-assisted Wireless Networks Using Mixture Gamma Model, International Conference on Innovative Mobile and Internet Services in Ubiquitous Computing" *Springer*, Cham, 2021: 168-178.
- [22] Y. Chen et al., "Downlink Performance Analysis of Intelligent Reflecting Surface-Enabled Networks," *IEEE Transactions on Vehicular Technology*, vol. 72, no. 2, pp. 2082-2097, Feb. 2023.
- [23] L. Yang, X. Li, S. Jin, M. Matthaiou and F. -C. Zheng, "Fine-Grained Analysis of Reconfigurable Intelligent Surface-Assisted mmWave Networks," *IEEE Transactions on Communications*, vol. 70, no. 9, pp. 6277-6294, Sept. 2022.
- [24] Stoyan D, Kendall W S, Chiu S N, et al, "Stochastic geometry and its applications," *John Wiley & Sons*, 2013.
- [25] Haenggi M, "Stochastic Geometry for Wireless Networks," *Cambridge University Press*, 2012.
- [26] J.-S. Ferenc and Z. Neda, "On the size distribution of poisson Voronoi cells," *Physica A: Statistical Mechanics and its Applications*, vol. 385, no. 2, pp. 518-526, 2007.
- [27] S. M. Yu and S. Kim, "Downlink capacity and base station density in cellular networks," *2013 11th International Symposium and Workshops on Modeling and Optimization in Mobile, Ad Hoc and Wireless Networks (WiOpt)*, pp. 119-124, 2013.
- [28] Gradshteyn I S, Ryzhik I M, "Table of integrals, series, and products," *Academic press*, 2014.
- [29] W. Wang and G. Shen, "Energy Efficiency of Heterogeneous Cellular Network," *2010 IEEE 72nd Vehicular Technology Conference - Fall*, Ottawa, ON, Canada, 2010, pp. 1-5.
- [30] G. Auer et al., "How much energy is needed to run a wireless network?," *IEEE Wireless Communications*, vol. 18, no. 5, pp. 40-49, October 2011.
- [31] Wang J, Tang W, Liang J C, et al, "Reconfigurable Intelligent Surface: Power Consumption Modeling and Practical Measurement Validation," *arXiv preprint arXiv:2211.00323*, 2022.